View metadata, citation and similar papers at core.ac.uk

brought to you by CORE

provided by Aston Publications Explorer

© 2016, Elsevier. Licensed under the Creative Commons Attribution-NonCommercial-NoDerivatives 4.0 International
http://creativecommons.org/licenses/by-nc-nd/4.0/

Phytochemical-loaded mesoporous silica nanoparticles for nose-to-brain olfactory drug delivery

Shital Lungare[1], Keith Hallam[2], Raj K. S. Badhan[1]

[1] Aston Pharmacy School, Life and Health Sciences, Aston University, Birmingham, B4 7ET, United Kingdom.

[2] Interface Analysis Centre, School of Physics, University of Bristol, Bristol BS8 1TL, United Kingdom.

Correspondence:

Dr Raj K. Singh Badhan
Aston Pharmacy School
Life and Health Sciences
Aston University
Birmingham
B4 7ET
UK
Telephone: +44 121 204 3288
Fax: +44 121 204 3000
E-mail: r.k.s.badhan@aston.ac.uk

ABSTRACT

Central nervous system (CNS) drug delivery is often hampered due to the insidious nature of the blood-brain barrier (BBB). Nose-to-brain delivery *via* olfactory pathways have become a target of attention for drug delivery due to bypassing of the BBB. The antioxidant properties of phytochemicals make them promising as CNS active agents but possess poor water solubility and limited BBB penetration. The primary aim of this study was the development of mesoporous silica nanoparticles (MSNs) loaded with the poorly water-soluble phytochemicals curcumin and chrysin which could be utilised for nose-to-brain delivery. We formulated spherical MSNP using a templating approach resulting in ~220 nm particles with a high surface porosity. Curcumin and chrysin were successfully loaded into MSNP and confirmed through Fourier transformation infrared spectroscopy (FT-IR), differential scanning calorimetry (DSC), thermogravimetric analysis (TGA) and HPLC approaches with a loading of 11-14% for curcumin and chrysin. Release was pH dependant with curcumin demonstrating increased chemical stability at a lower pH (5.5) with a release of 53.2 % ± 2.2 % over 24 hours and 9.4 ± 0.6 % for chrysin. MSNP were demonstrated to be non-toxic to olfactory neuroblastoma cells OBGF400, with chrysin (100 µM) demonstrating a decrease in cell viability to 58.2 ± 8.5 % and curcumin an IC_{50} of 33 ± 0.18 µM. Furthermore confocal microscopy demonstrated nanoparticles of < 500nm were able to accumulate within cells with FITC-loaded MSNP showing membrane localised and cytoplasmic accumulation following a 2-hour incubation. MSNP are useful carriers for poorly soluble phytochemicals and provide a novel vehicle to target and deliver drugs into the CNS and bypass the BBB through olfactory drug delivery.

KEYWORDS

Mesoporous silica nanoparticle; olfactory; nose-to-brain; flavonoid; phytochemical.

*Graphical Abstract (for review)

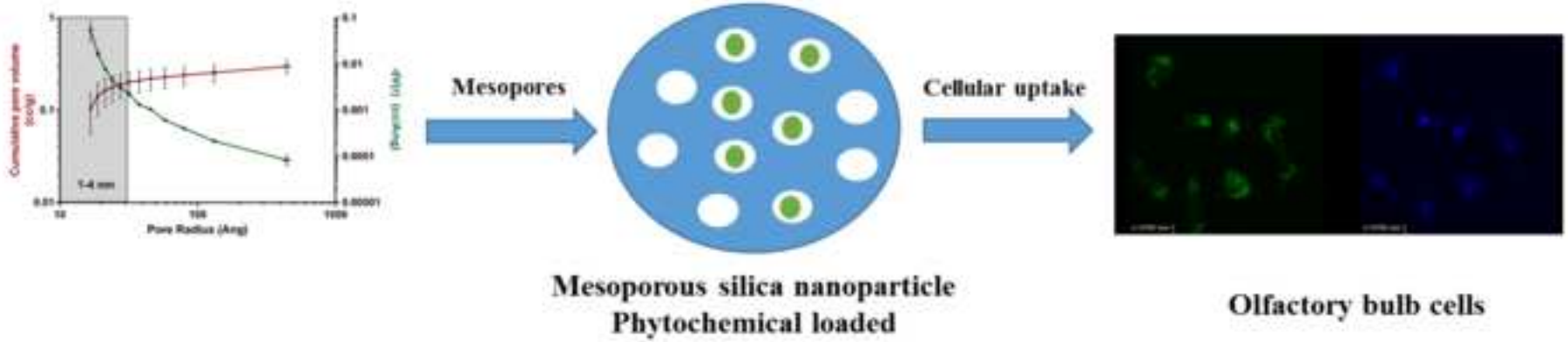

1. INTRODUCTION

The World Health Organisation (WHO) have highlighted that neurological disorders are one of the biggest threats to public health [1]. Disorders of the CNS account for approximately 1 % of deaths but this is associated with a worldwide disease burden of almost 11 %, and it is thought that approximately 1.5 billion people worldwide suffer from some kind of brain or CNS disorder [1]. Furthermore with an increasingly ageing population, by the year 2020 one in every three people alive will suffer from a central nervous system (CNS) related disorder [1].

Similar paradigms exist within the pharmaceutical industry with less than 8 % of CNS-indicated drugs successfully enter clinical trials and accompanied by an overall drop in the success rate of delivering a candidate to market [2], with the US Food and Drug Administration (FDA) only approving between 15-25 new compounds per year [2]. Despite advances in drug delivery technologies, CNS drug targeting and delivery is still a limiting factor with less than 1 % of all CNS-targeted compounds showing activity against CNS diseases [3, 4]. This is despite many of these compounds possessing physicochemical properties that would normally predispose them to good membrane permeability (e.g, molecular weight < 500 and highly lipid soluble) [5]. The brain is a very highly vascularised organ with a microvascular surface area of 150-200 cm^2 g. tissue (12-18 m^2) in humans [6]. However, the primary cause of poor brain deposition of therapeutics is often associated with an impermeable barrier termed the blood-brain barrier (BBB), formed from brain microvascular endothelial cells and which are highly selective in controlling the entry of endogenous and exogenous compounds into the brain.

The development of CNS disorders is often associated with the process of oxidative stress and leads to a range of neurological disorders such as epilepsy [7], Alzheimer's disease and dementia [8]. However, a novel category of potential therapeutic agents possessing anti-oxidant activities are phytochemicals, which are derived from natural extracts from plants. Over 8000 compounds have been identified as belonging to the general category of polyphenols [9] of which flavonoids are a major class and contributing over 6500 distinct compounds [10].

Many phytochemicals have been reported to possess CNS indicating effects including the protection of neurons from neurotoxins and neuro-inflammation in degenerative diseases [11-17]. Furthermore, an increasing body of clinical evidence is supporting the view that flavonoids impart a protective function towards dopamine neurons through the prevention of oxidative damage and apoptosis [18, 19]. The target site for flavonoids is thought to be widespread within the CNS, but much attention has been focussed on the ability of phytochemicals to interact with the $GABA_A$ receptor, one of the most important neurotransmitter sites within the CNS. Indeed, many phytochemicals demonstrated significant inhibitory actions on $GABA_A$ in low micromolar concentration, e.g. chrysin (3 μM) [20] and 6-methylapigenin (495 nM) [21]. Furthermore, chrysin has been demonstrated to result in anxiolytic in mice at an intraperitoneal dose of 1 mg/kg [22]. In addition to their action on receptor sites, a range of phytochemicals have been demonstrated to modulate the genome and proteome of the promiscuous network of membrane transporter proteins localised at the BBB [23].

Phytochemical flavonoids are therefore a potentially novel multi-faceted class of molecules which show potential for a range of CNS patho-physiologies [24-36]. However, many phytochemicals are poorly soluble and are not immediately amenable to direct formulation into dosage forms for oral/transdermal or parenteral systems.

Many groups have demonstrated successful loading and delivery of phytochemicals using nanoparticle carrier systems to enhance their solubility and delivery, with the most commonly studied phytochemical being curcumin [37-40] and chrysin [41, 42, 43]

A class of biocompatible nanomaterials that has gained attention for drug delivery are mesoporous silica nanoparticles (MSNP). Silica is biocompatible and is often used in inorganic nanoparticles [44, 45]. Silica nanoparticles are highly porous in nature, with the pore sizes, density and total surface area being highly tuneable making them excellent tools for biomolecule detection, drug delivery systems and for contrast agent protectors [46-48]. Mesoporous material was first discovered by Mobil Corporation in 1992 [49] and termed MCM-41, possessing a honeycomb-like porous structure with hundreds of pore channels (termed mesopores) that have the potential to absorb molecules . This results in mesoporous nanoparticles having a high surface area (> 900 m^2/g), large pore volume (> 0.9 cm^3/g) with the added benefit of a tuneable pore size over a very narrow size distribution (2–10 nm) [50]. Furthermore, mesoporous silica nanoparticles have recently been used to demonstrate loading and release of curcumin [51].

To overcome the difficulties associated with crossing the BBB, approaches at bypassing the BBB have more recently focused on exploiting the olfactory mucosa within the nasal cavity, by virtue of the fact that olfactory neurones are directly exposed to the external environment [52, 53] and provide a direct pathway to the olfactory bulb and brain. This regions covers the upper part of the nasal cavity with an approximate surface area of 2.5-10 cm^2 in humans [54]. It is primarily comprised of approximately 12 million olfactory receptor cells [55]. The olfactory region has been the focus of one of the major 'nose-to-brain' pathways to deliver drugs directly to the brain through olfacotry deposition. The first recorded success in the delivery of a therapeutic agent into the brain in humans, following IN administration, was in a patent application by William Frey II [56, 57] reporting the successful delivery of neurological agents and macromolecules (insulin) [58] targeting Alzheimer's disease. These reports established a novel approach to target CNS drug delivery through potential bypassing of the BBB, and is particularly attractive as the targeted delivery onto the olfactory mucosa (as opposed to parenteral delivery) would require reduced drug loaded requirements.

Given the relative ease of preparation of MSNP and the tuneable nature of the nanomaterials, MSNP are an interesting group of nanoparticles which have not fully been exploited for nose-to-brain delivery. The aim of this study is to investigate the use of MSNP as carriers for the poorly soluble phytochemicals curcumin and chrysin, which are known to possess CNS pharmacological action [59-68], and to assess their loading capacity and release profile along with the cellular compatibility and *in-vitro* uptake into cultured olfactory cells.

2. MATERIALS AND METHODS

2.1 Materials

Dulbecco's Modified Eagle Medium (MEM), Dulbecco's Modified Medium: Nutrient Mixture F12 (DMEM-F12), Dulbecco's Phosphate buffered saline (PBS), L-glutamine 200mM, non-essential amino acids (NEAA), penicillin/streptomycin and trypsin-EDTA solution were obtained from PAA laboratories (Austria); foetal bovine serum (FBS) (Labtech, Essex, UK); potassium chloride, magnesium sulphate, calcium chloride, acetonitrile, orthophosphoric acid, acetic acid, ethanol, sodium hydroxide, and sodium chloride were obtained from Fisher Scientific (Loughborough, UK); acutase (Biolegend, UK); gentamycin, cetyl trimethylammonium bromide (CTAB), tetraethoxy orthosilicate (TEOS), (3-(4, 5-dimethylthiazol-2-yl)-2, 5-diphenyl Tetrazolium bromide) MTT, trypan blue, dimethyl

sulfoxide (DMSO), potassium phosphate, ammonium hydroxide, rhodamine 6G, fluorescein isothiocynate (FITC),DAPI, collagen, cell culture water, monobasic were obtained from Sigma-Aldrich (Dorset, UK).

2.2 Methods

2.2.1 Preparation of MSNP

MSNP were prepared using a modified method described by Fan et al [69]. Briefly, 1.0 g of CTAB (2.74 mmol) was dissolved in 480 mL distilled water. Thereafter 3.5 mL of aqueous sodium hydroxide solution (2 M) was added and the temperature of the mixture was raised to 80 °C. 5 mL TEOS (22.4 mmol) was then introduced drop wise into the reaction mixture whilst stirring vigorously for two hours until a white precipitate was formed. The precipitate was then filtered and washed with distilled water and methanol and dried under vacuum. The surfactant template (CTAB) was removed by refluxing 1.5 g of the synthesized silica particles with 1.5 mL of hydrochloric acid (37.2 % w/v) and 150 mL methanol for 6 hours. The product was washed extensively with distilled water and methanol. The surfactant free silica particles were placed under high vacuum with heating at 60°C to remove the remaining solvent from the mesopores.

2.2.2 Size and zeta-potential

The size and zeta potential (ζ) of MSNPs were determined using dynamic light scattering techniques through the use of a NanoBrook 90 Plus Zeta (Brookhaven Instruments Corporation). 100 µL of 1 mg/mL sonicated MSNPs suspension was added to 3 mL ultrapure water, vortexed and used to measure the particles size. The mean diameter was obtained from 3 runs of 3 minutes. The polydispersity index (PDI) was used to indicate the particle size distribution within the sample. The zeta potential is an indicator for charge present on the surface of nanoparticles, which is responsible for the stability of formulation and interaction with cellular membranes. The zeta potential of nanoparticles is measured using the principle of electrophoretic mobility under an electric field. The average of 3 readings (each reading = 30 runs) was reported. The temperature was maintained at 25°C during the measurements.

2.2.3 SEM

Samples of MSNP were mounted on 12 mm aluminium pin stubs with 12 mm carbon tabs and coated with 15nm of gold. The powders were imaged at 5 kV with a 150 pA beam in high vacuum due to beam damage to the samples at higher kV's. The nanoparticles were imaged at 10 kV with a 100 pA beam also in high vacuum using a Carl Zeiss EVO LS 15 with a Quorum QR105S gold coater.

2.2.4 Nitrogen absorption-desorption

The specific surface areas of the blank MSNPs were analysed using the Brunauer–Emmet–Teller (BET) method [70] using a Quantchrome NOVA (Quantchrom, Finland). The analysis was based on the amount of Nitrogen (N_2) gas adsorbed at various partial pressures (P/P0) between 0.05 and 0.3. Before N_2 adsorption, samples were degassed under vacuum at a temperature of 100° C. The nitrogen molecular cross sectional area (0.162 nm^2) was used to determine the surface area. The pore size distribution and total pore volume was determined by using density functional theory (DFT) method. All calculations were software automated (Quantchrome NOVAWIN, Quantchrom, Finland).

2.2.5 TGA

Thermal stability analysis of the functionalized silica was performed by thermogravimetric analysis (TGA) using a Pyris 1 TGA (Perkin Elmer) instrument. 3 mg of MSNP materials were analyzed under nitrogen purge with a starting temperature of 35 °C and 10 °C/min ramp rate to 800 °C. The corresponding carbon, hydrogen and nitrogen elemental analysis was performed using a LECO CHN-2000 elemental analyzer under flowing oxygen.

2.2.6 DSC

Heating curves of MSNP were obtained using differential scanning calorimeter (DSC Q200, TA instruments, Delware). Samples were weighed and 2-5 mg were loaded into a non-hermetically crimped aluminium pan and heated under a nitrogen purge at the rate 50 mL/min. Samples were heated from 30 to 350°C at the heating rate 10°C/min under nitrogen. Data was analysed using Universal Analysis 2000 software V4.5A TA instruments.

2.2.7 FT-IR

MSNP were further characterised by using FT-IR techniques for the bare MSNPs, and drug loaded MSNPs. FT-IR absorbance was collected using a Nicolet iS5 FT-IR spectrophotometer (Thermo Scientific,USA) over the spectral range of 550-4000 cm^{-1}.

2.2.8 Phytochemical loading

Chrysin: 20 mg/mL chrysin was dissolved in DMF and in a separate vial 20 mg/mL of MSNPs were dispersed in DMF and bath sonicated for 15 minutes. A volume of 1 mL from each vial was combined and resulted in a final concentration of 10 mg/mL of both chrysin and MSNP. The glass vial was sealed and covered with foil, sonicated for 15 minutes in a water sonicating bath and left for stirring at 100 rpm at room temperature. After 24 hours the vial contents was filtered through a 0.22 µm cellulosic white membrane filter (MSI Micron Separations Inc., USA). Chrysin loaded MSNP were termed ‘Chry-MSNP’.

Curcumin: 20 mg/mL curcumin was dissolved in a 30:70 mixture acetone:ethanol and processed as described above. Curcumin loaded MSNP were termed ‘Curc-MSNP’.

The filtrate was collected to determine the loading (entrapment efficiency) and this approach was termed the ‘wet’ approach. The entrapment efficiency (EE) was calculated based on the following formula:

$$\text{EE}\ (\%) = \frac{\text{Compound added} - \text{Free "unentrapped compound"}}{\text{Compound added}} \times 100$$

where HPLC-UV methods were used to assess content.

The loaded nanoparticles collected on the filter paper were dried under high vacuum for 2 days, washed with PBS to remove superficially adsorbed phytochemicals and loading was assessed through TGA. This approach was termed the ‘dry’ approach, where the loading content (LC) was calculated from the difference between the final weight loss for MSNP and phytochemical loaded MSNP at the end of the heating cycle and derived from data obtain from TGA analysis.

Confirmation of phytochemical loading was further determined using HPLC-UV, DSC, TGA, FT-IR and DLS/zeta potential analysis.

2.2.9 Cellular toxicity towards olfactory cells: MTT assay

To assess the compatibility between formulation and olfactory mucosa type cells, the porcine olfactory bulb neuroblastoma cell line OBGF400 was used as an *in-vitro* cell culture model of the olfactory cells/mucosa [71]. OBGF400 cells are bipolar to multipolar in nature with prominent cell bodies and a distinctive nucleus and extending axonal structures confirm as neuronal cells.

OBGF400 were a kind gift from Dr. Gail Scherba (University of Illinois, USA) and were grown in DMEM/F-12 (Dulbecco's Modified Medium: Nutrient Mixture F12) supplemented with sodium bicarbonate, HEPES, gentamicin (50 µg/mL), penicillin G/streptomycin, bovine calf serum (BCS) in a humidified 37°C incubator with 5% CO_2. At 80-90 % confluency, the media was aspirated and cells were treated with Acutase® for 20-30 minutes prior to passaging.

Cells were seeded into 96-well plates at a density of $1x10^4$ cells per well. Cells were subsequently exposed to 10-1000 µg/mL MSNPs for 24 hours at 37 °C and 5 % CO_2 humidified environment and cellular toxicity was assessed using a 3-(4,5-Dimethylthiazol-2-yl)-2,5-Diphenyltetrazolium Bromide (MTT) assay. Briefly, following incubation the media was removed and replaced with 100 µL of media containing 0.5 mg/mL MTT dissolved in PBS and incubated at 37 °C in an air humidified environment for 4 hours. Thereafter, the media was removed and 100 µL of DMSO was added and the plates left to incubate for 15 minutes in the dark. The UV-absorbance of the formazan product was determined at 595 nm.

The UV-absorbance of the formazan product was measured on a multi-plate reader (Bio-Rad laboratories, Hercules, CA) using 570 nm as a test wavelength and 600 nm as a reference wavelength. The mean of the blank UV-absorbance was subtracted from the UV-absorbance of each controls and samples and percentage viability was calculated as follows:

$$\%\ \text{cell viability} = \frac{\text{absorbance of sample}}{\text{absorbance of control}} * 100$$

The cellular viability IC_{50} was subsequently calculated using a sigmoidal dose response function. Each concentration was assayed in eight wells and run in three independent experiments and results expressed as percentage cytotoxicity relative to a control (0.5% DMSO).

The cellular toxicity of curcumin and chrysin were also assessed using OBGF 400 cells at a concentration range of 0.01-50,000 µM, as described above. The cell viability was calculated by comparing the absorbance of phytochemical or drug treated well to that of control well.

2.2.10 Cellular toxicity towards olfactory cells: Live cell imaging

To assess the morphological alterations in cellular structures when exposed to MSNP, Curc-MSNP and Chry-MSNP, live cell imaging of OBGF400 was conducted over a 40-hour period in an oxygen, CO_2 and humidity controlled phase contrast imaging systems (CellIQ®, Chip-Man Technologies, Tampere, Finland). OBGF400 cells were seeded into wells of a 6-well plate at a density of $5x10^5$ cells/well and allowed to adhere and proliferate to 70 % confluence. Subsequently wells were washed with warm HEPES (25 mM) buffered HBSS, followed by the addition of 50-150 µg/mL of MSNP, Curc-MSNP and Chry-MSNP dispersed

in maintenance media for 40 hours with images captured within a defined window within each well every 15 minutes using live-cell imaging and presented as images.

2.2.11 Cellular uptake of nanoparticles into olfactory cells

Coverslips were sterilised in 70% ethanol for 30 minutes, dried in a laminar air hood and coated with 6 µg/cm^2 of a collagen prepared in sterile water from a 0.1 % w/v (0.1 M acetic acid) stock solution, with coating taking place in 12-well plates. Plates were left to dry in the laminar air flow for 2 hours. Excess collagen was then removed and coverslips washed with sterile water and left for drying. Thereafter cell suspensions of OBGF 400 cells were seeded at a density of 1x10^5 cells/cm^2 into wells of a 12 well plate containing the coated coverslips and left to adhere and proliferate to a confluency of approximately 70% in a 5% CO_2 humidified incubator.

To identify the optimal particle size range for olfactory uptake, fluorescent latex beads (carboxylate modified) of 100 nm (λ_{ex} ~491 nm; λ_{em} ~521 nm) and 500 nm (λ_{ex} ~575 nm; λ_{em} ~610 nm) were initially utilised as a rapid fluorescence-based screening tool to consider the boundary range of 100-500 nm for nanoparticle uptake into OBGF400 cells. Fluorescent latex beads were dispersed into HEPES (25mM) buffered HBSS at a concentration of 0.1 % v/v and sonicated for 10 minutes in a water-bath sonicator prior to the addition into wells. Subsequently, to assess the cellular uptake of formulated MSNP (section 2.2.1), FITC was passively loaded into MSNP (see supplementary materials section 1), dispersed into HEPES (25mM) buffered HBSS at a concentration of 0.1 % v/v and sonicated for 10 minutes in a water-bath sonicator prior to the addition into wells

Coverslips were incubated for 2 hours in a 5 % CO_2 humidified incubator before being washed with ice cold HEPES (25mM) buffered HBSS and fixed with 4 % w/v paraformaldehyde for 30 minutes in the dark. The coverslips were then mounted onto glass slides with mounting media containing 4',6-diamidino-2-phenylindole (DAPI). The localisation of the latex beads was analysed using an upright confocal microscope (Leica SP5 TCS II MP) and visualised with a 40x oil immersion objective. All images were acquired using an argon laser at 494 nm or DPSS 561 laser at 561 nm to visualise beads/MSNP and a helium laser to visualise DAPI at 461 nm.

2.2.12 HPLC detection of phytochemicals

The detection of curcumin was based on an adapted method previously reported by Li et al [72]. An Agilent 1200 Series (Waldbronn, Germany) equipped with a multiple wavelength detector (MWD) and a Phenomenex Luna C18 (150 × 4.6 mm) 5 µm column was used for RP-HPLC. The mobile phase was prepared using ACN:5% acetic acid in a ratio of 45: 55 (v/v). Mobile phases were filtered through a 0.45 µm filter and sonicated before use. The flow rate was maintained at 0.8 mL/min with a 15 minutes run time and injection volume of 20 µL, while column temperature was mainlined at ambient temperatures. Calibration curves were constructed using standard solutions of known concentrations from 5 to 50 µg/mL. The software used for data collection, analysis and control of the system was ChemStation Version 1.24 SP1. The UV detection of curcumin was measured at 420 nm.

An RP-HPLC method was used to quantify chrysin [73]. The same HPLC system described above was used to analyse chrysin samples. The mobile phase comprised of water:methanol:acetonitrile:phosphoric acid in a ratio of 60:30:38:1 (v/v). Mobile phases were filtered through 0.45 µm filter and sonicated before use. The flow rate was maintained at 1.0 mL/min with 17 minutes run time and the injection volume was 10 µL while column temperature was kept at ambient temperatures. Calibration curves were constructed using

standard solutions of known concentrations from 0.78 to 10,000 µg/mL. The UV detection of chrysin was measured at 262 nm.

2.2.13 Release of phytochemicals from MSNP

To assess the *in-vitro* release of curcumin and chrysin from MSNPs, studies were performed in phosphate buffered saline (154 mM PBS pH 7.4) containing 0.1 % Tween 80. Phytochemical loaded MSNP, 2 mg, were dispersed into 2 mL of release medium, briefly sonicated and placed in a shaking incubator maintained at 37 ˚C and 100 rpm. Samples were withdrawn at set time intervals and the volume replaced with an equal volume of pre-warmed release medium. The release of phytochemicals was assessed through HPLC-UV methods. Throughout the release studies Tween 80 was used to maintain the sink conditions and also to dissolve curcumin in the release medium [74]. The results were calculated in terms of cumulative release (% w/w) relative to actual entrapped weight of curcumin or chrysin in the MSNPs. To assess the impact of pH on drug release, release studies were also conducted at pH 5.5 (average nasal pH).

2.2.14 Statistical analysis

Unless otherwise stated, three independent experiments were carried out for each study. Statistical significance was evaluated by one-way ANOVA or paired two-tail Students t-test using GraphPad Prism version 6.00 (GraphPad Software, La Jolla California USA, www.graphpad.com). Unless otherwise stated, data is reported as mean ± standard deviation (SD). A significance level (P-value) of < 0.05 was considered as statistically significant.

3. RESULTS AND DISCUSSION

3.1 MSNP formulation and characterisation

MSNP were formulated according to the methods described by Fan et al [69], which employs a templating approach where template removal determines the hollow interior of the MSNP. During the formation CTAB is responsible for the formation of the shell and TEOS determines the hollow interior of the MSNPs [75].

Synthesis of MSN yielded particle sizes of 216.5 ± 2.1 nm with a PDI of 0.13 ± 0.02 and a zeta-potential of -23.9 ± 0.4 (Figure 1A), similar to that reported by Fan et (180-185 nm). To confirm the particle size of the formulated MSNP, SEM imaging was used to assess the morphological structure of MSNP. The nanoparticles developed demonstrated a uniform particle distribution of similar sizes and relatively uniform smooth particles and particle sizes of approximately 200 nm (Figure 1B and 1C).

FT-IR assessment was also used to assess the removal of the template from the mesoporous materials and confirmed with four bands at 550, 1500, 2900 and 3000 cm^{-1} before CTAB removal (Figure 2) corresponding to the CH_2 and CH_3 groups in CTAB molecule structure, which were eliminated after template removal (Figure 2).

To determine the porosity of the MSNP and ascertain the pore volume and density, nitrogen adsorption/desorption isotherms were generated. The nitrogen absorption-desorption isotherms identify the characterise hysteresis-type loop associated with capillary (pore) condensation at $P/P_0 > \approx 0.2$ (Figure 3A). The hysteresis loop can be classified as a H1 loop, which is often associated with porous materials exhibiting a narrow distribution of relatively uniform (cylindrical-like) pores. The overall distribution of the pore radius was confirmed

through BJH analysis and demonstrated a narrow pore radius relative to the cumulative pore volume with the majority of the radius distribution, dV(r), located <20-30 Ang (< 10 nm). Furthermore, the pore width distribution confirmed a pore with distribution of < 4 nm (Figure 3B and C) with a large surface area 987.67 ± 3.38 m^2/g and the DFT method confirms that the average pore size of 1.93 ± 0.01 nm (Figure 3B and C) with total pore volume 0.95 ± 0.004 cc/g and possessing similar porosity to other reported MSNP [76, 77].

3.2 Phytochemical loading into MSNP

The loading of curcumin into MSNP was confirmed through FT-IR analysis. The characteristic IR absorption frequencies in the spectral range of 550-4000 cm^{-1} were measured for free curcumin and Curc-MSNPs. The interaction between MSNPs and curcumin after being loading was also analysed using FTIR. Curcumin spectra shows the following characteristic peaks: broad peak at 3420 cm^{-1} confirming the intermolecular hydrogen bonding in isolated silanol and enolic hydroxyl groups, with a broader shift when incorporated into MSNP indicating potential enhancement of hydrogen boding (Figure 4A). The signature peaks of curcumin are located at 1627 cm^{-1} and 1602 cm^{-1} and are attributed to the C═C double bonds and aromatic C═C double bonds, respectively [78] (Figure 4B). Finally bands at 1,279 cm^{-1} and 1,152 cm^{-1} were assigned to the aromatic C-O stretching and stretching in the C-O-C [78] (Figure 4B) [79, 80]. In all cases, these bands were absent in the blank MSNP. For chrysin, the FT-IR spectrum shows bands at 2921 cm^{-1}, 2710 cm^{-1} and 2631 cm^{-1} for stretching in the C-H and C=C (Figure 4C and D). Furthermore, carbonyl group vibrations coupled with the double band in the γ-benzopyrone ring at 1653 cm^{-1} and absorption bands at 1612, 1577 and 1450 cm^{-1} related to carbon vibration in benzene and γ - pyrone rings (valance vibrations C=C) can be observed (Figure 4D) [81].

To further characterise the loading of phytochemicals into MSNP, DSC thermographs were analysed for blank and loaded MSNP. The thermograms of pure curcumin and chrysin show characteristic single melting endothermic peak at 176°C (Figure 5A) and 286 °C respectively (Figure 5B), which were absent in the loaded MSNP (Figure 5A). Furthermore, the absence of characteristic single melting endothermic peaks for loaded MSNP confirms the washing step in the 'dry method' had removed residual phytochemical adsorbed onto the surface of the MSNPs and secondly that the loaded phytochemical was present in the amorphous form.

Furthermore, TGA analysis show that the total weight loss of the loaded MSNP at the end of the run was 22.16 ± 1.12 % compared to the blank MSNPs, 7.21 ± 0.45 % with a calculated LC of 14.95 ± 0.67 % and which corresponds to the calculated EE of 12.34 ± 1.28 % for the 'wet method' for curcumin (Figure 5C). For chrysin the total weight loss of the Fan-MSNP at the end of the run was 21.07 ± 0.75 % compared to the blank MSNPs, 9.58 ± 1.94 % with a calculated LC of 11.49 ± 1.19 % and which corresponds to the calculated EE of 12.34 ± 1.28 % for the 'wet method' (Figure 5D).

To confirm loading of curcumin into MSNP, particle size demonstrating an increase in the hydrodynamic mean diameter from 216.8 ± 2.1 nm to 263.51 ± 8.3 nm after loading with curcumin ($P \leq 0.01$) with a statistically significant increase in the PDI from 0.13 ± 0.02 to 0.26 ± 0.05 ($P \leq 0.05$) (Figure 6A). Furthermore the zeta potential of the Curc-MSNP decreased from -23.9 ± 0.4 mV to -16.9 ± 0.9 mV ($P \leq 0.01$) (Figure 6B). This increase in particle size and PDI has been previously reported after loading curcumin in their mesoporous nanoparticles [51, 79]. Furthermore the decrease in zeta potential following loading has previously been reported, however the polarity of the resultant charge is a function of the pH of the media that the zeta potential is measured in, with reports that a lower pH media often leads to more positive zeta potential with loading [82-85].

Similarly for chrysin the hydrodynamic mean diameter increased from 216.8 ± 2.1 nm to 283.5 ± 8.3 nm after loading ($P \leq 0.01$) with a statistically significant increase in the PDI from 0.13 ± 0.02 to 0.31 ± 0.11 ($P \leq 0.05$) (Figure 6C) and an associated decrease in zeta potential from -23.9 ± 0.4 mV to -30.8 ± 0.3 mV ($P \leq 0.01$) (Figure 6D). However reports from other chrysin loaded nanoparticle systems indicate a negative zeta potential in the range we detected [86, 87].

Traditionally the zeta potential has been considered an important element for cellular interaction, with positively charged NP being favoured over negatively charges NP due to the negative charge of a cell membrane [88]. That said, a number of reports have identified that the zeta potential is less of an issue for MSNP due to their highly mesoporous nature [89 90]. Furthermore the endosome escaping, "proton sponge" effect [91], may explain the ability of Fan-MSNP to undergo internalisation, considering negative charge, without any specific ligands for receptor mediated endocytosis.

With TGA analysis some weight loss at low temperature may have been attributed to adsorbed water whereas the weight loss at higher temperatures can be attributed to loss of surface silanol groups. However, no significant weight loss was evident during the study and this implies Fan-MSNP were thermally stable [92]. In the case of both chrysin and curcumin, the loaded nanoparticles demonstrated no characteristic melting point depression confirming the amorphous nature of the loaded phytochemical and confirming negligible drug adsorbed [93].

3.3 Cellular toxicity towards olfactory cells

To investigate the toxicity of MSNP, curcumin and chrysin towards OBGF400 cells a cell viability assay was conducted with phytochemicals/MSNP exposed to OBGF400 for 24 hours. For MSNP, cell viability was generally maintained across the concentration range of 10-100 µg/mL (Figure 7A), with a statistically significant ($P \leq 0.01$) decrease in viability from 100 µg/mL onwards. For curcumin (Figure 7B) and chrysin (Figure 7C), cell viability was maintained across the concentration range of 0.001-10 µM and an IC_{50} of 33 ± 0.18 µM was determined for curcumin. For chrysin at 100 µM, a statistically significant ($P \leq 0.01$) decrease in cell viability was observed (to 58.2 ± 8.5 %). Reports of toxicity of MSNP with olfactory cells have not been reported by others but contradictory reports comment on relationships between the particle size and cellular toxicity, which appears to be cell line specific. For example, smaller-sized silica nanoparticles induced severe cellular damage in lung cancer cells, myocardial cells, and human endothelial cells [94-96] and this was thought to be related to the fact that smaller nanoparticles have larger ratio of surface area to weight and therefore potentially more contact with the cells to induce damage [97-99]. However others have reported that larger silica nanoparticles are more cytotoxic than smaller particles on human hepatoma cells [100].

All MTT assays were conducted in cell culture media containing serum. A possible explanation for the conflicting reports in cellular toxicity associated with MSNP (and NP more generally) may be associated with a protein corona that is formed on the surface of silica nanoparticles that may alter the cytotoxic potential of the nanoparticles when in contact with serum proteins from tissue culture media [101, 102].

No other reports are available of the cellular toxicity of curcumin or chysin with OBGF400 cells, however others have reported similar IC_{50} in CNS related cell lines (porcine brain microvascular endothelial cells PBMEC/C1-2: 63 ± 1.2 µM) [23]. Similar IC_{50} values have been reported for curcumin, 15.2 µM and 16.4 µM against A2780CP and MDA-MB-231 cells

respectively [74]. Mukerjee and Vishwanatha [103] found the IC_{50} of curcumin loaded PLGA nanoparticle was 31µM for PWR 1E cells as compared to 37µM of free curcumin

Any foreign particle to be taken up by the cell is dependent upon many factors such as size, charge, affinity etc. It has been reported that nanoparticles smaller than 100 nm could cause unspecific cellular uptake and cytotoxicity [104]. Silica nanoparticles in the size range of 50-300 nm are capable of inducing endocytosis [105] without causing any cytotoxicity and they have been reported to possess high affinity to many phospholipids present on the surface of the cell, which may even induce pinocytosis [106].

To assess the morphological alteration of cellular structures when exposed to MSNP, Curc-MSNP and Chry-MSNP, a gas and humidity controlled phase contrast imaging study was conducted using the CellIQ® imaging system. OBGF400 cells, grown in wells of a 6-well plates, were exposed to 50-150 µg/mL of MSNP, Curc-MSNP and Chry-MSNP for 40 hours with images captures within a defined window within each well every 15 minutes using live-cell imaging. The impact of MSNP on cell viability/proliferation at 150 µL/mL demonstrate a clear impact on the viability and proliferation of OBGF400 over 40 hours resulting in a reduction in the cell morphological volume and cell death. This effect was diminished at a concentration of 50 µg/mL, where cell morphology was maintained throughout the incubation period (See supplementary materials figure 2)

With Chry-MSNP, a similar impact on cell viability was noted at 150 µg/mL. However, at 50 µg/mL cell morphology was seen to change associated with the apoptosis of some cells (See supplementary materials figure 3). For Curc-MSNP, cell morphology was noted to alter at 150 µg/mL leading to an increase in cell death over time, however at 50 µg/mL cell viability was not affected and proliferation of cells was noted (See supplementary materials figure 4).

3.4 Cellular uptake of nanoparticles into olfactory cells

A key goal for our studies was to demonstrate uptake of MSNP into olfactory bulb neuronal cells. To assess this process fluorescent latex beads of 100 nm and 500 nm size ranges were selected to allow cellular imaging of the intracellular localisation of beads, providing some insight into appropriate size ranges for viable cellular uptake. For 100 nm sized latex beads the cellular localisation of the beads is evident, particularly in the membrane regions and cytoplasm (Figure 8). For the 500 nm sized latex beads a x63 magnification was used to enlarge isolated OBGF400 cells with membrane localisation and partial cytoplasmic trapping observed (Figure 8).

The fluorescent molecule FITC was subsequently passively loaded into MSNP resulting in an EE of 48 ± 2.3 % and the release of FITC was assessed in PBS (pH 7.4) media (See supplementary materials). The duration of the release study was set at 2 hours, primarily as a result of the short exposure-time expected with nasally delivered formulation coupled with the limited duration with which cell cultures can proliferate in the absence of growth media. Minimal FITC was identified as having been released from FITC-MSNP, 4.8 ± 0.19 %, over a 2-hour period suggesting the relative stability of the FITC molecule within the MSNP structure (see supplementary materials Figure 1).

To further discern the exact localisation of MSNP within the cell, FITC loaded MSNP were prepared and incubated with OBGF400 cells before z-stack confocal microscopy was used to capture FITC- MSNP fluorescence through the z-dimension of the cell The confocal stage was set at the upper-most boundary of the OBGF 400 cells and the stage moved down towards the coverslip with images captured over a z-dimension of approximately 5 µm. At the onset of the z-stack analysis, FITC-MSNP is localised on the exterior of the cell boundary

and potentially on the surface of the cells (10763 µm). As the stage progresses, the localisation of FITC-MSNP increases with clear demarked zones of cytoplasmic localisation near the 'mid-to-bottom' regions of the cells (Figure 9).

However, cellular uptake of both sizes of beads were detected using confocal microscopy and suggest MNSP formulation over this size range would be appropriate for olfactory uptake. Although the use of fluorescent latex beads as retrograde transport markers for neuronal pathways is not new [107-109], the application to olfactory bulb neuronal cells is novel indicates the potential for nano-sized material to penetrate into this class of cells.

MSNP possessing a negative zeta potential have been previously reported [110-112] and associated with successful cellular uptake for both naïve MSNP and modified MSNP. The uptake of MSNP in our study is presumed to be through a nonspecific pathway as the use of naïve MSNP incorporated no surface functionalisation for cellular targeting. Furthermore, the location of clarithin coated vesicles on olfactory and the reported uptake of MSNP via clathrin-dependent endocytotic pathways due to their siliceous composition, and unique hexagonal exterior and internal hexagonal mesopores[113] would indicated this would be the favoured uptake route of otherwise electronically unfavourable interactions between MSNP and the cell membrane. Furthermore, the it has been reported that nanoparticles possess a negative zeta potential illicit a "proton sponge" effect within the endosome whereby the negative zeta potential MSNP would aid in buffering the internal charge of the endosome, resulting in an increase in osmotic pressure (due to Cl- influx) and swelling and finally facilitating endosomal escape through rupturing[91].

3.5 Phytochemical release study from the mesoporous silica nanoparticles

The release of curcumin from Curc-MSNP was assessed over 24 hours and demonstrated a pH sensitive release phenomena. A burst effect was also evident after 1 hour with 12 % and 16.6 % released at pH 7.4 and pH 5.5 respectively (Figure 10A). Release at pH 7.4 was slower than that at pH 5.5, with 16.1 ± 1.6 % released at 24 hours ($P \leq 0.001$). At pH 5.5 release increased over 24 hours to 53.2 % ± 2.2 % ($P \leq 0.001$). However, no significant increase in curcumin release was observed from 1 hour to 24 hours.

The release of chrysin from Chry-MSNP was assessed over 24 hours and also demonstrated a pH sensitive release phenomena. A burst effect was evident after 1 hour with 3.2 ± 1.2 % and 7.1 ± 1.6 % released at pH 7.4 and pH 5.5 respectively (Figure 10B). Release at pH 5.5 was slower than that for pH 7.4 ($P \leq 0.001$), with 9.4 ± 0.6 % and 16.8 ± 0.8 % at 24 hours respectively. However statistically significant differences ($P \leq 0.001$) were also observed between 1 hour and 24 hours release at each pH studied. Furthermore, the release profile for both phytochemicals demonstrated a burst effect at early time points and this pattern has also been reported elsewhere [114-117]. This may be a result of the rapid dissolution of the loaded phytochemicals closer to the exterior of the pores with slower penetration of solvent into the pores as a result of the micro/meso size pores of < 2 nm .

The differences in release of curcumin from mesoporous nanoparticles at difference pHs is important as the release in the nasal cavity (pH 5.5) is likely to be more rapid. Furthermore, it has been reported that curcumin is relatively unstable at pH 7.4 compared to more acidic pH, which may explain the lack of increase in cumulative release from 1 hour to 24 hours (~1.8 %) compared to the ~36% increase in cumulative release at pH 5.5 at 24 hours [117-119].

The degradation has been reported to be complex but at a pH < 1, curcumin exists in the protonated form (H_4A^+), with increasing pH the neutral form (H_3A) predominates. Furthermore stability in acidic conditions is likely due to its conjugated diene structure which becomes gradually destroyed as the proton is removed during the dissociation of the phenolic groups within the structure of curcumin (H_2A^-, HA^{2-} and A^{3-}) which occurs at higher pHs and is likely the cause of curcumin being significantly more prone to degradation [120, 118]. An analysis of the HPLC chromatograms for curcumin at 1 hour and 24 hour also confirms differences in peak ratios suggesting degradation of curcumin at pH 7.4 rather than pH 5.5 (See supplementary materials figure 5).

Therefore at nasal pH (~5.5) both curcumin and chrysin loaded MSNP would be expected to be relatively stable at physiological pH and undergo release from the MSNP.

The difference in cumulative release between phytochemicals may be related to the pore size. The pore size influences the potential loading capacity (and therefore potentially the release pattern) from MSNP [106,121]. Furthermore, the penetration of the phytochemicals within the naïve (non-functionalised) pores of MSNP would largely therefore depend on the molecular properties of the loaded phytochemicals.

Curcumin posses a larger molecular weight (368.38 g/mol) and 3 distinct molecular entities: two aromatic ring systems containing o-methoxy phenolic groups, connected with a seven carbon linker consisting of an α,β-unsaturated β-diketone structure with the diketo group exhibiting keto-enol tautomerism. Chrysin (254.23 g/mol) on the other hand belongs to the flavone group of phytochemicals and consists of A and C rings, and a phenyl B ring attached to position 2 of the C ring, thus essentially three pi-pi conjugated rings. As a result of the narrow pore width, the difference in release rates may be a function of the ability of curcumin to diffuse from within the porous structure more rapidly (due to steric hindrances) compared to chrysin. Furthermore chrysin possess planar stereochemistry and the pi-pi structure would enhance the non-covalent bonding interactions within the pores, resulting in a slower release profile.

4. CONCLUSION

Age related neurological disorders such as Parkinson's disease (PD) and Alzheimer's disease (AD), are insidious progressive neurological disorders which are expected to increase in incidence over the next century. Current approaches to CNS drug delivery are often hampered by poor targeting and drug delivery to the BBB and nose-to-brain delivery, following olfactory targeting, provides a promising novel way to bypass the BBB.

We have developed phytochemical-loaded MSNP and have systemically investigated the loading, uptake and *in-vitro* release of phytochemicals from MSNP. Our studies have demonstrated that nanoparticles below 500 nm would be capable of being taken up by olfactory cells and that the release of phytochemicals from MSNP is pH dependant, potentially suited to the slightly acidic nature of the nasal cavity.

Although the successful intranasal delivery of the formulation onto the olfactory mucosa may significantly enhance its eventual delivery to the brain, we believe that the present study demonstrates the benefits of MSNP as a drug carrier and particularly in its applications towards nose-to-brain delivery of phytochemical loaded nano-carriers.

ACKNOWLDEGMENTS

The authors would like to thank Aston University for providing the Overseas Student Scholar Scheme to fund this project. We would also like to acknowledge Aston Research Centre for Healthy Ageing and Charlotte Bland for assisting with the collection of confocal imaging data.

REFERENCES

1. WHO, *Neurological Disorders: Public Health Challenges*. World Health Organization: 2006.
2. Kola, I.; Landis, J. Can the pharmaceutical industry reduce attrition rates? *Nat Rev Drug Discov* **2004,** *3*, (8), 711-5.
3. Pardridge, W. M. The blood-brain barrier: bottleneck in brain drug development. *NeuroRx* **2005,** *2*, (1), 3-14.
4. Lipinski, C. A. Drug-like properties and the causes of poor solubility and poor permeability. *J Pharmacol Toxicol Methods* **2000,** *44*, (1), 235-49.
5. Pardridge, W. M. CNS drug design based on principles of blood-brain barrier transport. *Journal of neurochemistry* **1998,** *70*, (5), 1781-92.
6. Abbott, N. J.; Romero, I. A. Transporting therapeutics across the blood-brain barrier. *Molecular Medicine Today* **1996,** *2*, (3), 106-113.
7. Diniz, T. C.; Silva, J. C.; de Lima-Saraiva, S. R.; Ribeiro, F. P.; Pacheco, A. G.; de Freitas, R. M.; Quintans-Junior, L. J.; Quintans Jde, S.; Mendes, R. L.; Almeida, J. R. The role of flavonoids on oxidative stress in epilepsy. *Oxid Med Cell Longev* **2015,** *2015*, 171756.
8. Bennett, S.; Grant, M. M.; Aldred, S. Oxidative stress in vascular dementia and Alzheimer's disease: a common pathology. *Journal of Alzheimer's disease : JAD* **2009,** *17*, (2), 245-57.
9. Pandey, K. B.; Rizvi, S. I. Plant polyphenols as dietary antioxidants in human health and disease. *Oxid Med Cell Longev* **2009,** *2*, (5), 270-278.
10. Kong, Y.; Ma, W.; Liu, X.; Zu, Y. G.; Fu, Y. J.; Wu, N.; Liang, L.; Yao, L. P.; Efferth, T. Cytotoxic Activity of Curcumin towards CCRF-CEM Leukemia Cells and Its Effect on DNA Damage. *Molecules (Basel, Switzerland)* **2009,** *14*, (12), 5328-5338.
11. Williams, R. J.; Spencer, J. P. Flavonoids, cognition, and dementia: actions, mechanisms, and potential therapeutic utility for Alzheimer disease. *Free Radic Biol Med* **2012,** *52*, (1), 35-45.
12. Solanki, I.; Parihar, P.; Mansuri, M. L.; Parihar, M. S. Flavonoid-based therapies in the early management of neurodegenerative diseases. *Adv Nutr* **2015,** *6*, (1), 64-72.
13. Shukitt-Hale, B. Blueberries and neuronal aging. *Gerontology* **2012,** *58*, (6), 518-23.
14. Mecocci, P.; Tinarelli, C.; Schulz, R. J.; Polidori, M. C. Nutraceuticals in cognitive impairment and Alzheimer's disease. *Front Pharmacol* **2014,** *5*, 147.
15. Macready, A. L.; Kennedy, O. B.; Ellis, J. A.; Williams, C. M.; Spencer, J. P.; Butler, L. T. Flavonoids and cognitive function: a review of human randomized controlled trial studies and recommendations for future studies. *Genes Nutr* **2009,** *4*, (4), 227-42.
16. Cherniack, E. P. A berry thought-provoking idea: the potential role of plant polyphenols in the treatment of age-related cognitive disorders. *Br J Nutr* **2012,** *108*, (5), 794-800.

17. Blumberg, J. B.; Ding, E. L.; Dixon, R.; Pasinetti, G. M.; Villarreal, F. The science of cocoa flavanols: bioavailability, emerging evidence, and proposed mechanisms. *Adv Nutr* **2014,** *5*, (5), 547-9.
18. Mercer, L. D.; Kelly, B. L.; Horne, M. K.; Beart, P. M. Dietary polyphenols protect dopamine neurons from oxidative insults and apoptosis: investigations in primary rat mesencephalic cultures. *Biochem Pharmacol* **2005,** *69*, (2), 339-45.
19. Meng, X.; Munishkina, L. A.; Fink, A. L.; Uversky, V. N. Molecular mechanisms underlying the flavonoid-induced inhibition of alpha-synuclein fibrillation. *Biochemistry* **2009,** *48*, (34), 8206-24.
20. Medina, J. H.; Paladini, A. C.; Wolfman, C.; de Stein, M. L.; Calvo, D.; Diaz, L. E.; Peña, C. Chrysin (5,7-di-OH-flavone), a naturally-occurring ligand for benzodiazepine receptors, with anticonvulsant properties. *Biochemical Pharmacology* **1990,** *40*, (10), 2227-2231.
21. Wasowski, C.; Marder, M.; Viola, H.; Medina, J. H.; Paladini, A. C. Isolation and identification of 6-methylapigenin, a competitive ligand for the brain GABA(A) receptors, from Valeriana wallichii. *Planta medica* **2002,** *68*, (10), 934-6.
22. Wolfman, C.; Viola, H.; Paladini, A.; Dajas, F.; Medina, J. H. Possible anxiolytic effects of chrysin, a central benzodiazepine receptor ligand isolated from Passiflora coerulea. *Pharmacology, biochemistry, and behavior* **1994,** *47*, (1), 1-4.
23. Kaur, M. Phytochemical Mediated Modulation Of Breast Cancer Resistance Protein At The Blood Brain Barrier And Blood Cerebrospinal Fluid Barrier. Aston University, 2016.
24. Katayama, K.; Masuyama, K.; Yoshioka, S.; Hasegawa, H.; Mitsuhashi, J.; Sugimoto, Y. Flavonoids inhibit breast cancer resistance protein-mediated drug resistance: transporter specificity and structure-activity relationship. *Cancer Chemother Pharmacol* **2007,** *60*, (6), 789-97.
25. Breedveld, P.; Beijnen, J. H.; Schellens, J. H. M. Use of P-glycoprotein and BCRP inhibitors to improve oral bioavailability and CNS penetration of anticancer drugs. *Trends in pharmacological sciences* **2006,** *27*, (1), 17-24.
26. Allen, J. D.; van Loevezijn, A.; Lakhai, J. M.; van der Valk, M.; van Tellingen, O.; Reid, G.; Schellens, J. H. M.; Koomen, G. J.; Schinkel, A. H. Potent and Specific Inhibition of the Breast Cancer Resistance Protein Multidrug Transporter in Vitro and in Mouse Intestine by a Novel Analogue of Fumitremorgin C 1 This work was supported in part by grant NKI 97-1433 from the Dutch Cancer Society (to AHS). Synthesis investigations by A. v. L. and GJ. K. were supported by the Netherlands Research Council for Chemical Sciences (NWO/CW) and the Netherlands Technology Foundation (STW). 1. *Molecular cancer therapeutics* **2002,** *1*, (6), 417-425.
27. Ashida, H.; Fukuda, I.; Yamashita, T.; Kanazawa, K. Flavones and flavonols at dietary levels inhibit a transformation of aryl hydrocarbon receptor induced by dioxin. *FEBS letters* **2000,** *476*, (3), 213-7.
28. Pick, A.; Müller, H.; Mayer, R.; Haenisch, B.; Pajeva, I. K.; Weigt, M.; Bönisch, H.; Müller, C. E.; Wiese, M. Structure–activity relationships of flavonoids as inhibitors of breast cancer resistance protein (BCRP). *Bioorganic & Medicinal Chemistry* **2011,** *19*, (6), 2090-2102.
29. Fleisher, B.; Unum, J.; Shao, J.; An, G. Ingredients in Fruit Juices Interact with Dasatinib Through Inhibition of BCRP: A New Mechanism of Beverage–Drug Interaction. *Journal of Pharmaceutical Sciences* **2015,** *104*, (1), 266-275.
30. Zhang, S.; Yang, X.; Morris, M. E. Flavonoids are inhibitors of breast cancer resistance protein (ABCG2)-mediated transport. *Molecular pharmacology* **2004,** *65*, (5), 1208-1216.

31. van Zanden, J. J.; van der Woude, H.; Vaessen, J.; Usta, M.; Wortelboer, H. M.; Cnubben, N. H. P.; Rietjens, I. M. C. M. The effect of quercetin phase II metabolism on its MRP1 and MRP2 inhibiting potential. *Biochemical pharmacology* **2007,** *74*, (2), 345-351.
32. Zhang, S.; Wang, X.; Sagawa, K.; Morris, M. E. Flavonoids chrysin and benzoflavone, potent breast cancer resistance protein inhibitors, have no significant effect on topotecan pharmacokinetics in rats or mdr1a/1b (-/-) mice. *Drug metabolism and disposition: the biological fate of chemicals* **2005,** *33*, (3), 341-8.
33. Robey, R. W.; Steadman, K.; Polgar, O.; Morisaki, K.; Blayney, M.; Mistry, P.; Bates, S. E. Pheophorbide a is a specific probe for ABCG2 function and inhibition. *Cancer research* **2004,** *64*, (4), 1242-1246.
34. Ferrandiz, M. L.; Alcaraz, M. J. Anti-inflammatory activity and inhibition of arachidonic acid metabolism by flavonoids. *Agents and actions* **1991,** *32*, (3-4), 283-8.
35. Breedveld, P.; Beijnen, J. H.; Schellens, J. H. Use of P-glycoprotein and BCRP inhibitors to improve oral bioavailability and CNS penetration of anticancer drugs. *Trends in pharmacological sciences* **2006,** *27*, (1), 17-24.
36. Allen, J. D.; van Loevezijn, A.; Lakhai, J. M.; van der Valk, M.; van Tellingen, O.; Reid, G.; Schellens, J. H.; Koomen, G. J.; Schinkel, A. H. Potent and specific inhibition of the breast cancer resistance protein multidrug transporter in vitro and in mouse intestine by a novel analogue of fumitremorgin C. *Molecular cancer therapeutics* **2002,** *1*, (6), 417-25.
37. Gupta, V.; Aseh, A.; Rios, C. N.; Aggarwal, B. B.; Mathur, A. B. Fabrication and characterization of silk fibroin-derived curcumin nanoparticles for cancer therapy. *International journal of nanomedicine* **2009,** *4*, 115-22.
38. Gupta, N. K.; Dixit, V. K. Development and evaluation of vesicular system for curcumin delivery. *Arch Dermatol Res* **2011,** *303*, (2), 89-101.
39. Gupta, N. K.; Dixit, V. K. Bioavailability enhancement of curcumin by complexation with phosphatidyl choline. *J Pharm Sci* **2011,** *100*, (5), 1987-95.
40. Krausz, A. E.; Adler, B. L.; Cabral, V.; Navati, M.; Doerner, J.; Charafeddine, R. A.; Chandra, D.; Liang, H.; Gunther, L.; Clendaniel, A.; Harper, S.; Friedman, J. M.; Nosanchuk, J. D.; Friedman, A. J. Curcumin-encapsulated nanoparticles as innovative antimicrobial and wound healing agent. *Nanomedicine: Nanotechnology, Biology and Medicine* **2015,** *11*, (1), 195-206.
41. Mohammadian, F.; Pilehvar-Soltanahmadi, Y.; Mofarrah, M.; Dastani-Habashi, M.; Zarghami, N. Down regulation of miR-18a, miR-21 and miR-221 genes in gastric cancer cell line by chrysin-loaded PLGA-PEG nanoparticles. *Artificial cells, nanomedicine, and biotechnology* **2016**, 1-7.
42. Zhu, Z. Y.; Luo, Y.; Liu, Y.; Wang, X. T.; Liu, F.; Guo, M. Z.; Wang, Z.; Liu, A. J.; Zhang, Y. M. Inclusion of chrysin in beta-cyclodextrin and its biological activities. *J Drug Deliv Sci Tec* **2016,** *31*, 176-186.
43. Chakraborty, S.; Basu, S.; Lahiri, A.; Basak, S. Inclusion of chrysin in beta-cyclodextrin nanocavity and its effect on antioxidant potential of chrysin: A spectroscopic and molecular modeling approach. *J Mol Struct* **2010,** *977*, (1-3), 180-188.
44. Bottini, M.; D'Annibale, F.; Magrini, A.; Cerignoli, F.; Arimura, Y.; Dawson, M. I.; Bergamaschi, E.; Rosato, N.; Bergamaschi, A.; Mustelin, T. Quantum dot-doped silica nanoparticles as probes for targeting of T-lymphocytes. *International journal of nanomedicine* **2007,** *2*, (2), 227-33.
45. Gerion, D.; Herberg, J.; Bok, R.; Gjersing, E.; Ramon, E.; Maxwell, R.; Kurhanewicz, J.; Budinger, T. F.; Gray, J. W.; Shuman, M. A.; Chen, F. F. Paramagnetic Silica-Coated Nanocrystals as an Advanced MRI Contrast Agent. *The Journal of Physical Chemistry C* **2007,** *111*, (34), 12542-12551.

46. Nehoff, H.; Parayath, N. N.; Domanovitch, L.; Taurin, S.; Greish, K. Nanomedicine for drug targeting: strategies beyond the enhanced permeability and retention effect. *International journal of nanomedicine* **2014,** *9*, 2539-2555.
47. Liao, Y.-T.; Liu, C.-H.; Yu, J.; Wu, K. C. Liver cancer cells: targeting and prolonged-release drug carriers consisting of mesoporous silica nanoparticles and alginate microspheres. *International journal of nanomedicine* **2014,** *9*, 2767.
48. Marzaioli, V.; Aguilar-Pimentel, J. A.; Weichenmeier, I.; Luxenhofer, G.; Wiemann, M.; Landsiedel, R.; Wohlleben, W.; Eiden, S.; Mempel, M.; Behrendt, H. Surface modifications of silica nanoparticles are crucial for their inert versus proinflammatory and immunomodulatory properties. *Int J Nanomed* **2014,** *9*, 2815-2832.
49. Kresge, C. T.; Leonowicz, M. E.; Roth, W. J.; Vartuli, J. C.; Beck, J. S. Ordered Mesoporous Molecular-Sieves Synthesized by a Liquid-Crystal Template Mechanism. *Nature* **1992,** *359*, (6397), 710-712.
50. Slowing, I. I.; Vivero-Escoto, J. L.; Wu, C.-W.; Lin, V. S. Y. Mesoporous silica nanoparticles as controlled release drug delivery and gene transfection carriers. *Advanced Drug Delivery Reviews* **2008,** *60*, (11), 1278-1288.
51. Kim, S.; Philippot, S.; Fontanay, S.; Duval, R. E.; Lamouroux, E.; Canilho, N.; Pasc, A. pH- and glutathione-responsive release of curcumin from mesoporous silica nanoparticles coated using tannic acid-Fe(III) complex. *RSC Advances* **2015,** *5*, (110), 90550-90558.
52. Illum, L. Transport of drugs from the nasal cavity to the central nervous system. *European journal of pharmaceutical sciences : official journal of the European Federation for Pharmaceutical Sciences* **2000,** *11*, (1), 1-18.
53. Pires, A.; Fortuna, A.; Alves, G.; Falcão, A. Intranasal drug delivery: how, why and what for? *Journal of Pharmacy & Pharmaceutical Sciences* **2009,** *12*, (3), 288-311.
54. Gizurarson, S. Anatomical and histological factors affecting intranasal drug and vaccine delivery. *Current drug delivery* **2012,** *9*, (6), 566-82.
55. Purves, D., *Neuroscience*. 4th ed. / edited by Dale Purves ... [et al.]. ed.; W. H. Freeman ; Basingstoke : Palgrave [distributor]: New York, 2007.
56. Frey, W. H. Method for administering neurologic agents to the brain. US 5624898 A, 1997.
57. Frey, W. H. Neurologic agents for nasal administration to the brain. WO1991007947 A1, 1997.
58. Frey, W. H. Method for administering insulin to the brain. US 6313093 B1, 2001.
59. Choudhury, D.; Ganguli, A.; Dastidar, D. G.; Acharya, B. R.; Das, A.; Chakrabarti, G. Apigenin shows synergistic anticancer activity with curcumin by binding at different sites of tubulin. *Biochimie* **2013,** *95*, (6), 1297-309.
60. Monroy, A.; Lithgow, G. J.; Alavez, S. Curcumin and neurodegenerative diseases. *Biofactors* **2013,** *39*, (1), 122-132.
61. Mythri, R. B.; Harish, G.; Dubey, S. K.; Misra, K.; Bharath, M. M. Glutamoyl diester of the dietary polyphenol curcumin offers improved protection against peroxynitrite-mediated nitrosative stress and damage of brain mitochondria in vitro: implications for Parkinson's disease. *Mol Cell Biochem* **2011,** *347*, (1-2), 135-43.
62. Zbarsky, V.; Datla, K. P.; Parkar, S.; Rai, D. K.; Aruoma, O. I.; Dexter, D. T. Neuroprotective properties of the natural phenolic antioxidants curcumin and naringenin but not quercetin and fisetin in a 6-OHDA model of Parkinson's disease. *Free Radical Res* **2005,** *39*, (10), 1119-1125.
63. Yao, Y.; Chen, L.; Xiao, J.; Wang, C.; Jiang, W.; Zhang, R.; Hao, J. Chrysin protects against focal cerebral ischemia/reperfusion injury in mice through attenuation of oxidative stress and inflammation. *International journal of molecular sciences* **2014,** *15*, (11), 20913-26.

64. Xiao, J.; Zhai, H.; Yao, Y.; Wang, C.; Jiang, W.; Zhang, C.; Simard, A. R.; Zhang, R.; Hao, J. Chrysin attenuates experimental autoimmune neuritis by suppressing immuno-inflammatory responses. *Neuroscience* **2014,** *262*, 156-64.
65. Souza, L. C.; Antunes, M. S.; Filho, C. B.; Del Fabbro, L.; de Gomes, M. G.; Goes, A. T.; Donato, F.; Prigol, M.; Boeira, S. P.; Jesse, C. R. Flavonoid Chrysin prevents age-related cognitive decline via attenuation of oxidative stress and modulation of BDNF levels in aged mouse brain. *Pharmacology, biochemistry, and behavior* **2015,** *134*, 22-30.
66. Santos, B. L.; Oliveira, M. N.; Coelho, P. L.; Pitanga, B. P.; da Silva, A. B.; Adelita, T.; Silva, V. D.; Costa Mde, F.; El-Bacha, R. S.; Tardy, M.; Chneiweiss, H.; Junier, M. P.; Moura-Neto, V.; Costa, S. L. Flavonoids suppress human glioblastoma cell growth by inhibiting cell metabolism, migration, and by regulating extracellular matrix proteins and metalloproteinases expression. *Chemico-biological interactions* **2015,** *242*, 123-38.
67. Nabavi, S. F.; Braidy, N.; Habtemariam, S.; Orhan, I. E.; Daglia, M.; Manayi, A.; Gortzi, O.; Nabavi, S. M. Neuroprotective effects of chrysin: From chemistry to medicine. *Neurochemistry international* **2015,** *90*, 224-31.
68. Jia, W. Z.; Zhao, J. C.; Sun, X. L.; Yao, Z. G.; Wu, H. L.; Xi, Z. Q. Additive anticancer effects of chrysin and low dose cisplatin in human malignant glioma cell (U87) proliferation and evaluation of the mechanistic pathway. *Journal of B.U.ON. : official journal of the Balkan Union of Oncology* **2015,** *20*, (5), 1327-36.
69. Fan, J.; Fang, G.; Wang, X.; Zeng, F.; Xiang, Y.; Wu, S. Targeted anticancer prodrug with mesoporous silica nanoparticles as vehicles. *Nanotechnology* **2011,** *22*, (45), 455102.
70. Brunauer, S.; Emmett, P. H.; Teller, E. Adsorption of Gases in Multimolecular Layers. *Journal of the American Chemical Society* **1938,** *60*, (2), 309-319.
71. Uebing-Czipura, A. U.; Dawson, H. D.; Scherba, G. Immortalization and characterization of lineage-restricted neuronal progenitor cells derived from the porcine olfactory bulb. *Journal of neuroscience methods* **2008,** *170*, (2), 262-76.
72. Li, J.; Jiang, Y.; Wen, J.; Fan, G.; Wu, Y.; Zhang, C. A rapid and simple HPLC method for the determination of curcumin in rat plasma: assay development, validation and application to a pharmacokinetic study of curcumin liposome. *Biomedical Chromatography* **2009,** *23*, (11), 1201-1207.
73. Zaveri, M.; Khandhar, A.; Jain, S. Quantification of baicalein, chrysin, biochanin-A and ellagic acid in root bark of Oroxylum indicum by RP-HPLC with UV detection. *Eurasian Journal of Analytical Chemistry* **2008,** *3*, (2), 245-257.
74. Yallapu, M. M.; Gupta, B. K.; Jaggi, M.; Chauhan, S. C. Fabrication of curcumin encapsulated PLGA nanoparticles for improved therapeutic effects in metastatic cancer cells. *J Colloid Interf Sci* **2010,** *351*, (1), 19-29.
75. Hao, N.; Jayawardana, K. W.; Chen, X.; Yan, M. One-step synthesis of amine-functionalized hollow mesoporous silica nanoparticles as efficient antibacterial and anticancer materials. *ACS applied materials & interfaces* **2015,** *7*, (2), 1040-1045.
76. He, Q.; Zhang, J.; Shi, J.; Zhu, Z.; Zhang, L.; Bu, W.; Guo, L.; Chen, Y. The effect of PEGylation of mesoporous silica nanoparticles on nonspecific binding of serum proteins and cellular responses. *Biomaterials* **2010,** *31*, (6), 1085-1092.
77. Wu, X.; Han, Z.; Schur, R. M.; Lu, Z.-R. Targeted Mesoporous Silica Nanoparticles Delivering Arsenic Trioxide with Environment Sensitive Drug Release for Effective Treatment of Triple Negative Breast Cancer. *ACS Biomaterials Science & Engineering* **2016,** *2*, (4), 501-507.
78. Feng, R.; Song, Z.; Zhai, G. Preparation and in vivo pharmacokinetics of curcumin-loaded PCL-PEG-PCL triblock copolymeric nanoparticles. *International journal of nanomedicine* **2012,** *7*, 4089-98.

79. Jambhrunkar, S.; Karmakar, S.; Popat, A.; Yu, M. H.; Yu, C. Z. Mesoporous silica nanoparticles enhance the cytotoxicity of curcumin. *Rsc Advances* **2014,** *4*, (2), 709-712.
80. Khan, M. A.; Akhtar, N.; Sharma, V.; Pathak, K. Product development studies on sonocrystallized curcumin for the treatment of gastric cancer. *Pharmaceutics* **2015,** *7*, (2), 43-63.
81. Zeng, Y. B.; Yang, N.; Liu, W. S.; Tang, N. Synthesis, characterization and DNA-binding properties of La(III) complex of chrysin. *J Inorg Biochem* **2003,** *97*, (3), 258-264.
82. Lee, C.-H.; Lo, L.-W.; Mou, C.-Y.; Yang, C.-S. Synthesis and Characterization of Positive-Charge Functionalized Mesoporous Silica Nanoparticles for Oral Drug Delivery of an Anti-Inflammatory Drug. *Advanced Functional Materials* **2008,** *18*, (20), 3283-3292.
83. Chung, T. H.; Wu, S. H.; Yao, M.; Lu, C. W.; Lin, Y. S.; Hung, Y.; Mou, C. Y.; Chen, Y. C.; Huang, D. M. The effect of surface charge on the uptake and biological function of mesoporous silica nanoparticles in 3T3-L1 cells and human mesenchymal stem cells. *Biomaterials* **2007,** *28*, (19), 2959-66.
84. DeMuth, P.; Hurley, M.; Wu, C.; Galanie, S.; Zachariah, M. R.; DeShong, P. Mesoscale porous silica as drug delivery vehicles: Synthesis, characterization, and pH-sensitive release profiles. *Micropor Mesopor Mat* **2011,** *141*, (1–3), 128-134.
85. Farghali, A.; Swiderska-Sroda, A.; Lojkowski, W.; Razin, A.-F. M.; Khedr, M.; AbouAitah, K. E. pH-controlled Release System for Curcumin based on Functionalized Dendritic Mesoporous Silica Nanoparticles. *Journal of Nanomedicine & Nanotechnology* **2016,** *2016*.
86. Wang, Z.; Fan, H.; Li, Y.; Wang, Y. Anti-hepatocarcinoma effects of chrysin loaded solid lipid nanoparticle against H22 tumor bearing mice. **2015**.
87. Sathishkumar, G.; Bharti, R.; Jha, P. K.; Selvakumar, M.; Dey, G.; Jha, R.; Jeyaraj, M.; Mandal, M.; Sivaramakrishnan, S. Dietary flavone chrysin (5,7-dihydroxyflavone ChR) functionalized highly-stable metal nanoformulations for improved anticancer applications. *RSC Advances* **2015,** *5*, (109), 89869-89878.
88. Cooper, G., *The Cell: A Molecular Approach. 2nd edition*. 2 ed.; Sinauer Associates: Sunderland (MA), 2000.
89. Taebnia, N.; Morshedi, D.; Doostkam, M.; Yaghmaei, S.; Aliakbari, F.; Singh, G.; Arpanaei, A. The effect of mesoporous silica nanoparticle surface chemistry and concentration on the alpha-synuclein fibrillation. *Rsc Advances* **2015,** *5*, (75), 60966-60974.
90. Huang, X. Y.; Young, N. P.; Townley, H. E. Characterization and Comparison of Mesoporous Silica Particles for Optimized Drug Delivery. *Nanomater Nanotechno* **2014,** *4*.
91. Boussif, O.; Lezoualch, F.; Zanta, M. A.; Mergny, M. D.; Scherman, D.; Demeneix, B.; Behr, J. P. A Versatile Vector for Gene and Oligonucleotide Transfer into Cells in Culture and in-Vivo - Polyethylenimine. *Proceedings of the National Academy of Sciences of the United States of America* **1995,** *92*, (16), 7297-7301.
92. Wanyika, H.; Gatebe, E.; Kioni, P.; Tang, Z. Y.; Gao, Y. Synthesis and characterization of ordered mesoporous silica nanoparticles with tunable physical properties by varying molar composition of reagents. *Afr J Pharm Pharmaco* **2011,** *5*, (21), 2402-2410.
93. Salonen, J.; Laitinen, L.; Kaukonen, A. M.; Tuura, J.; Bjorkqvist, M.; Heikkila, T.; Vaha-Heikkila, K.; Hirvonen, J.; Lehto, V. P. Mesoporous silicon microparticles for oral drug delivery: Loading and release of five model drugs. *Journal of Controlled Release* **2005,** *108*, (2-3), 362-374.
94. Napierska, D.; Thomassen, L. C.; Rabolli, V.; Lison, D.; Gonzalez, L.; Kirsch-Volders, M.; Martens, J. A.; Hoet, P. H. Size-Dependent Cytotoxicity of Monodisperse Silica Nanoparticles in Human Endothelial Cells. *Small* **2009,** *5*, (7), 846-853.
95. Ye, Y.; Liu, J.; Chen, M.; Sun, L.; Lan, M. In vitro toxicity of silica nanoparticles in myocardial cells. *Environmental toxicology and pharmacology* **2010,** *29*, (2), 131-137.

96. Lin, W.; Huang, Y.-w.; Zhou, X.-D.; Ma, Y. In vitro toxicity of silica nanoparticles in human lung cancer cells. *Toxicology and applied pharmacology* **2006,** *217*, (3), 252-259.
97. Oberdörster, G.; Oberdörster, E.; Oberdörster, J. Nanotoxicology: an emerging discipline evolving from studies of ultrafine particles. *Environmental health perspectives* **2005**, 823-839.
98. Kipen, H. M.; Laskin, D. L. Smaller is not always better: nanotechnology yields nanotoxicology. *American Journal of Physiology-Lung Cellular and Molecular Physiology* **2005,** *289*, (5), L696-L697.
99. Nel, A.; Xia, T.; Mädler, L.; Li, N. Toxic potential of materials at the nanolevel. *Science (New York, N.Y.)* **2006,** *311*, (5761), 622-627.
100. Lu, X.; Qian, J.; Zhou, H.; Gan, Q.; Tang, W.; Lu, J.; Yuan, Y.; Liu, C. In vitro cytotoxicity and induction of apoptosis by silica nanoparticles in human HepG2 hepatoma cells. *International journal of nanomedicine* **2011,** *6*, 1889-1901.
101. Barrett, E. G.; Johnston, C.; Oberdörster, G.; Finkelstein, J. N. Silica binds serum proteins resulting in a shift of the dose-response for silica-induced chemokine expression in an alveolar type II cell line. *Toxicology and applied pharmacology* **1999,** *161*, (2), 111-122.
102. Cedervall, T.; Lynch, I.; Foy, M.; Berggård, T.; Donnelly, S. C.; Cagney, G.; Linse, S.; Dawson, K. A. Detailed identification of plasma proteins adsorbed on copolymer nanoparticles. *Angewandte Chemie* **2007,** *119*, (30), 5856-5858.
103. Mukerjee, A.; Vishwanatha, J. K. Formulation, characterization and evaluation of curcumin-loaded PLGA nanospheres for cancer therapy. *Anticancer research* **2009,** *29*, (10), 3867-75.
104. Yu, K. O.; Grabinski, C. M.; Schrand, A. M.; Murdock, R. C.; Wang, W.; Gu, B. H.; Schlager, J. J.; Hussain, S. M. Toxicity of amorphous silica nanoparticles in mouse keratinocytes. *J Nanopart Res* **2009,** *11*, (1), 15-24.
105. Mayor, S.; Pagano, R. E. Pathways of clathrin-independent endocytosis. *Nat Rev Mol Cell Bio* **2007,** *8*, (8), 603-612.
106. Slowing, I. I.; Vivero-Escoto, J. L.; Wu, C. W.; Lin, V. S. Y. Mesoporous silica nanoparticles as controlled release drug delivery and gene transfection carriers. *Advanced Drug Delivery Reviews* **2008,** *60*, (11), 1278-1288.
107. Katz, L. C.; Burkhalter, A.; Dreyer, W. J. Fluorescent latex microspheres as a retrograde neuronal marker for in vivo and in vitro studies of visual cortex. *Nature* **1984,** *310*, (5977), 498-500.
108. Persson, H. G.; Gatzinsky, K. P. Distribution of retrogradely transported fluorescent latex microspheres in rat lumbosacral ventral root axons following peripheral crush injury: a light and electron microscopic study. *Brain Research* **1993,** *630*, (1–2), 115-124.
109. Katz, L. C.; Iarovici, D. M. Green fluorescent latex microspheres: A new retrograde tracer. *Neuroscience* **1990,** *34*, (2), 511-520.
110. Huang, X.; Teng, X.; Chen, D.; Tang, F.; He, J. The effect of the shape of mesoporous silica nanoparticles on cellular uptake and cell function. *Biomaterials*, **2010**, *31*, (3), 438-448.
111. Ma, X.; Teh, C.; Zhang, Q.; Borah, P.; Choong, C.; Korzh, V.; Zhao, Y. Redox-Responsive Mesoporous Silica Nanoparticles: A Physiologically Sensitive Codelivery Vehicle for siRNA and Doxorubicin. *Antioxidants & Redox Signaling* **2013**, *21*, (5), 707-722.
112. Meng, H.; Xue, M.; Xia, T.; Zhao, Y.-L.; Tamanoi, F.; Stoddart, J. F.; Zink, J.I.; Nel, A. E. Autonomous in Vitro Anticancer Drug Release from Mesoporous Silica Nanoparticles by pH-Sensitive Nanovalves. *Journal of the American Chemical Society* **2010,** *132*, (36), 12690-12697.
113. Huang, D. M.; Hung, Y.; Ko, B. S.; Hsu, S. C.; Chen, W. H.; Chien, C. L.; Tsai, C. P.; Kuo, C. T.; Kang, J. C.; Yang, C. S.; Mou, C. Y.; Chen, Y. C. Highly efficient cellular

labeling of mesoporous nanoparticles in human mesenchymal stem cells: implication for stem cell tracking. *Faseb Journal* **2005,** *19*, (12), 2014-6.
114. Anitha, A.; Deepagan, V. G.; Divya Rani, V. V.; Menon, D.; Nair, S. V.; Jayakumar, R. Preparation, characterization, in vitro drug release and biological studies of curcumin loaded dextran sulphate–chitosan nanoparticles. *Carbohydrate Polymers* **2011,** *84*, (3), 1158-1164.
115. Zou, P.; Helson, L.; Maitra, A.; Stern, S. T.; McNeil, S. E. Polymeric Curcumin Nanoparticle Pharmacokinetics and Metabolism in Bile Duct Cannulated Rats. *Molecular Pharmaceutics* **2013,** *10*, (5), 1977-1987.
116. Yin, H.; Zhang, H.; Liu, B. Superior anticancer efficacy of curcumin-loaded nanoparticles against lung cancer. *Acta Biochimica et Biophysica Sinica* **2013**.
117. Wang, Y. J.; Pan, M. H.; Cheng, A. L.; Lin, L. I.; Ho, Y. S.; Hsieh, C. Y.; Lin, J. K. Stability of curcumin in buffer solutions and characterization of its degradation products. *J Pharm Biomed Anal* **1997,** *15*, (12), 1867-76.
118. Tonnesen, H. H.; Karlsen, J. Studies on curcumin and curcuminoids. VI. Kinetics of curcumin degradation in aqueous solution. *Z Lebensm Unters Forsch* **1985,** *180*, (5), 402-4.
119. Kunnumakkara, A. B.; Anand, P.; Aggarwal, B. B. Curcumin inhibits proliferation, invasion, angiogenesis and metastasis of different cancers through interaction with multiple cell signaling proteins. *Cancer letters* **2008,** *269*, (2), 199-225.
120. Lee, W. H.; Loo, C. Y.; Bebawy, M.; Luk, F.; Mason, R. S.; Rohanizadeh, R. Curcumin and its derivatives: their application in neuropharmacology and neuroscience in the 21st century. *Current neuropharmacology* **2013,** *11*, (4), 338-78.
121. Gao, Y.; Chen, Y.; Ji, X.; He, X.; Yin, Q.; Zhang, Z.; Shi, J.; Li, Y. Controlled intracellular release of doxorubicin in multidrug-resistant cancer cells by tuning the shell-pore sizes of mesoporous silica nanoparticles. *ACS Nano* **2011**, *5*, (12), 9788-9798.

LIST OF FIGURES

Figure 10: Cumulative percentage release of (A) curcumin and (B) chrysin from MSNP. The *in vitro* release was performed in 154 mM PBS pH 7.4 and pH 5.5 containing 0.1 % Tween 80. 1 mg/mL of phytochemical loaded MSNP were dispersed into 2 mL of release medium, briefly sonicated and placed in a shaking incubator maintained at 37 ˚C and 100 rpm. Samples were withdrawn at set time intervals and the volume replaced with an equal volume of pre-warmed release medium. Release was assessed through HPLC-UV methods. N=3. # # # indicates statistical comparison between the final time point (24 hours) and the first time point for (1 hour) for pH 5.5 with a $P \leq 0.001$. *** indicates statistical comparison between the final time point (24 hours) between pH 5.5 and 7.4 with a $P \leq 0.001$

Figure 1

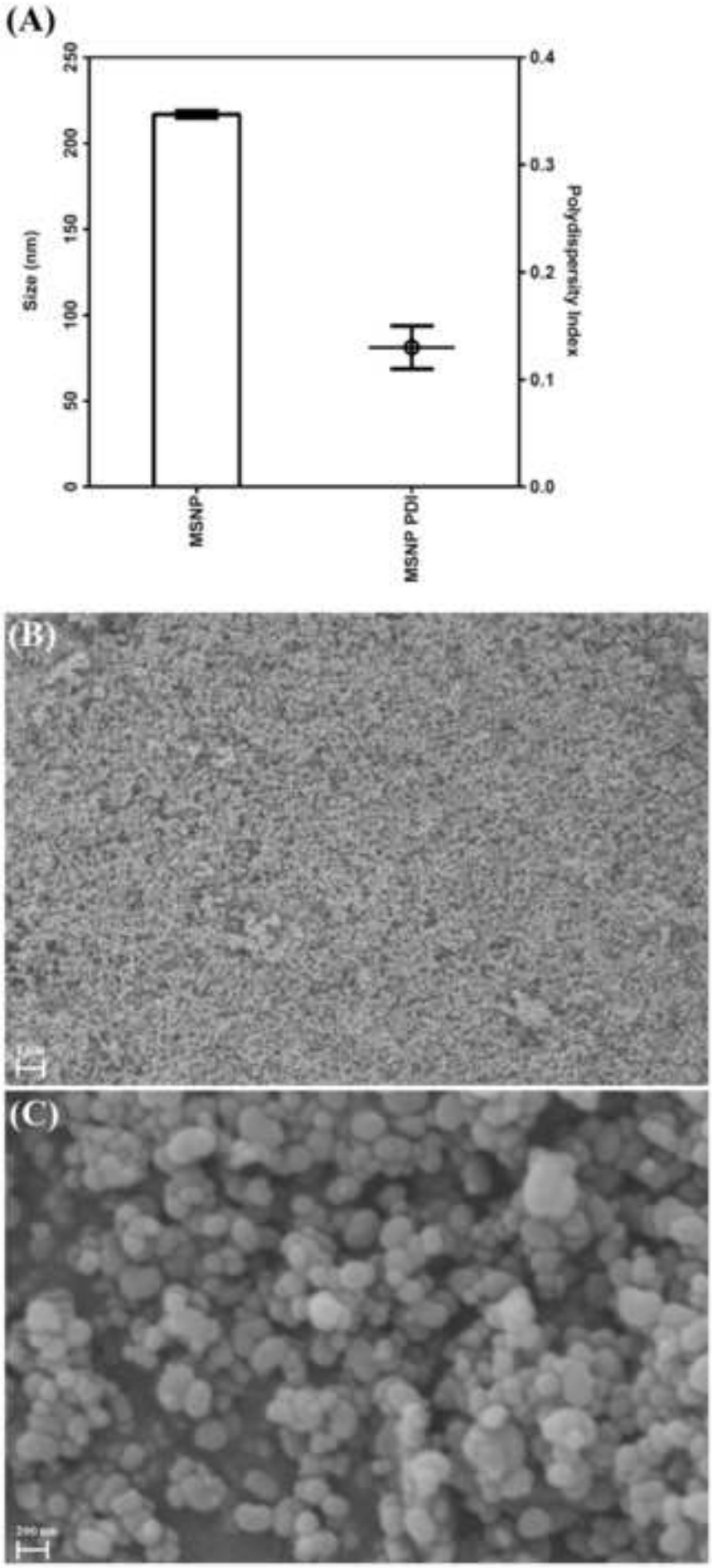
(A)
Size (nm)
Polydispersity Index
0
50
100
150
200
250
0.0
0.1
0.2
0.3
0.4
MSNP
MSNP PDI
(B)
(C)

Figure 2

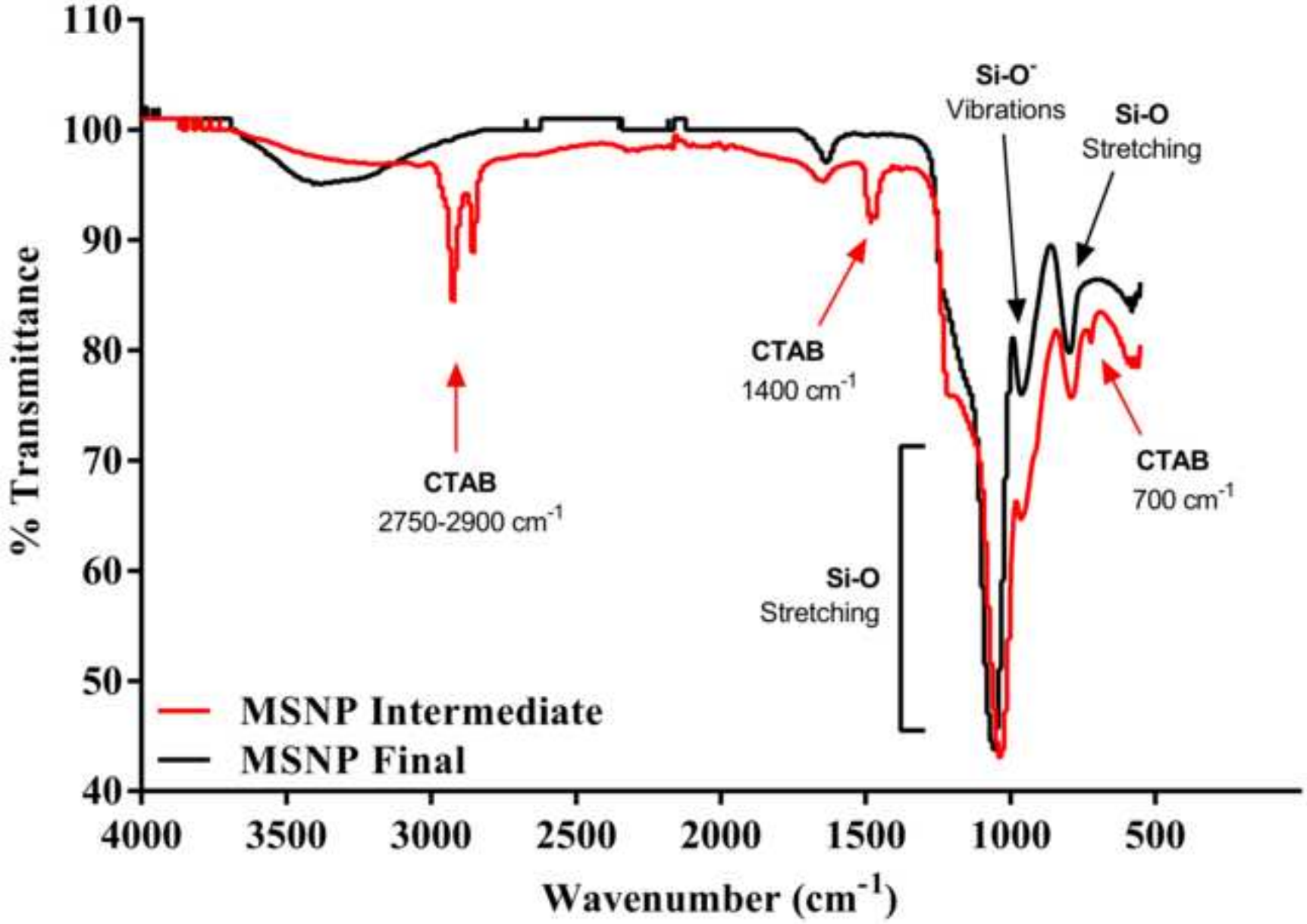
110
100
90
80
70
60
50
40
% Transmittance
4000
3500
3000
2500
2000
1500
1000
500
Wavenumber (cm-1)
MSNP Intermediate
MSNP Final
CTAB
2750-2900 cm-1
CTAB
1400 cm-1
Si-O-
Vibrations
Si-O
Stretching
Si-O
Stretching
CTAB
700 cm-1

Figure 3

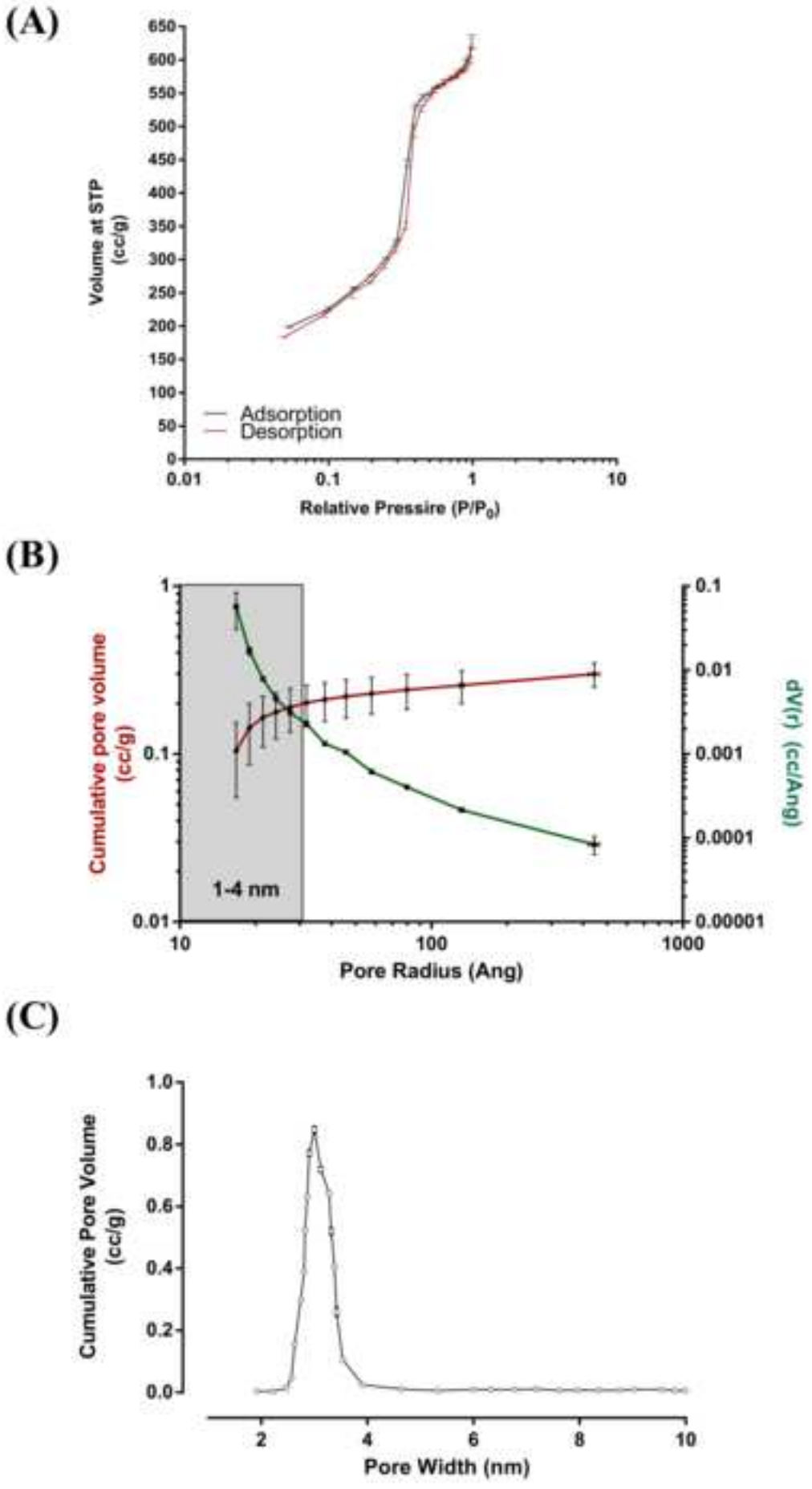
(A)
Volume at STP (cc/g)
650
600
550
500
450
400
350
300
250
200
150
100
50
0
0.01
0.1
1
10
Relative Pressire (P/P0)
Adsorption
Desorption
(B)
Cumulative pore volume (cc/g)
1
0.1
0.01
1-4 nm
10
100
1000
Pore Radius (Ang)
0.1
0.01
0.001
0.0001
0.00001
dV(r) (cc/Ang)
(C)
Cumulative Pore Volume (cc/g)
1.0
0.8
0.6
0.4
0.2
0.0
2
4
6
8
10
Pore Width (nm)

Figure 4

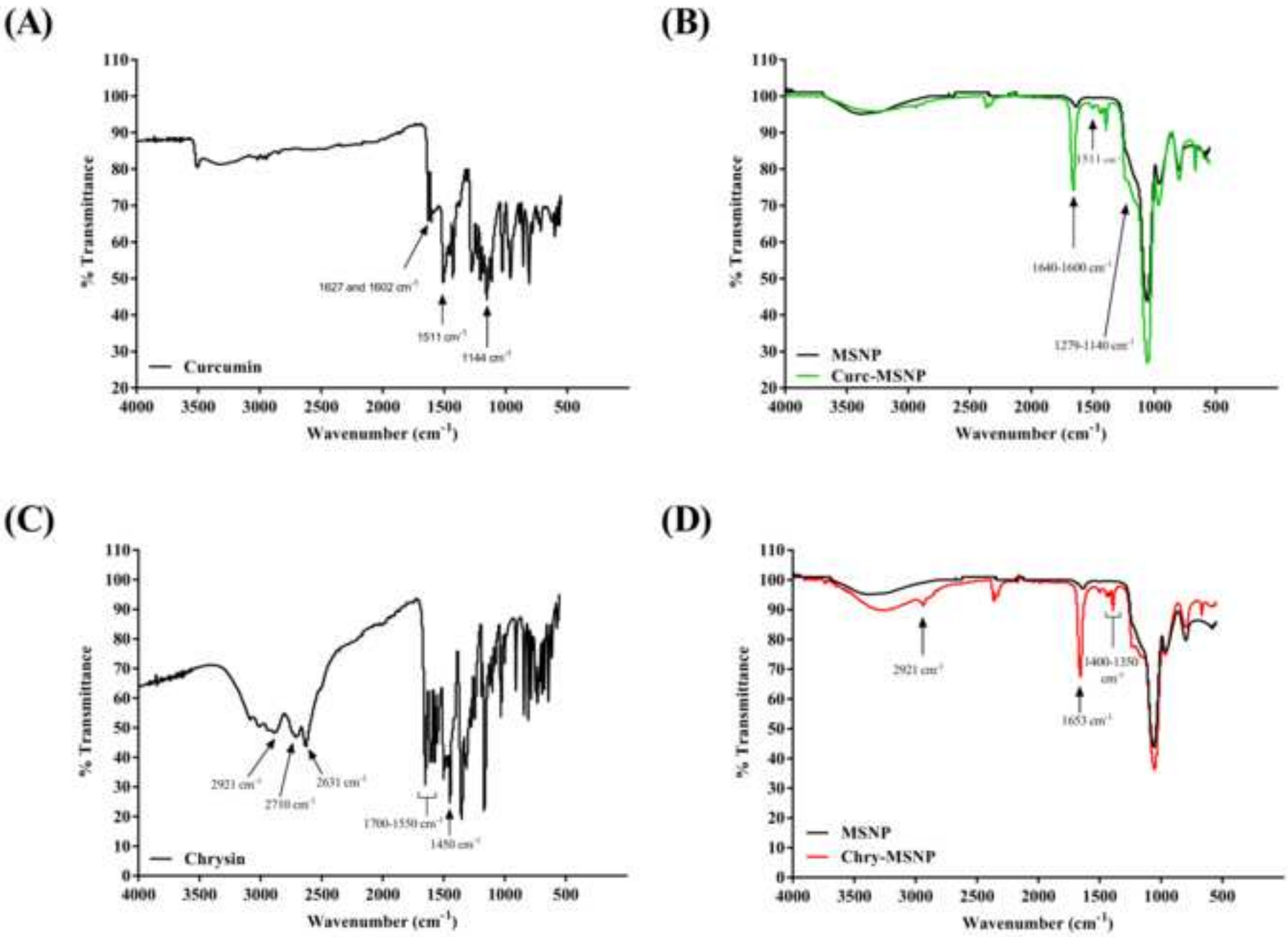
(A)
% Transmittance
Wavenumber (cm-1)
Curcumin
1627 and 1602 cm-1
1511 cm-1
1144 cm-1
(B)
% Transmittance
Wavenumber (cm-1)
MSNP
Curc-MSNP
1640-1600 cm-1
1279-1140 cm-1
(C)
% Transmittance
Wavenumber (cm-1)
Chrysin
2921 cm-1
2710 cm-1
2631 cm-1
1700-1550 cm-1
1450 cm-1
(D)
% Transmittance
Wavenumber (cm-1)
MSNP
Chry-MSNP
2921 cm-1
1653 cm-1
1400-1350 cm-1

Figure 5

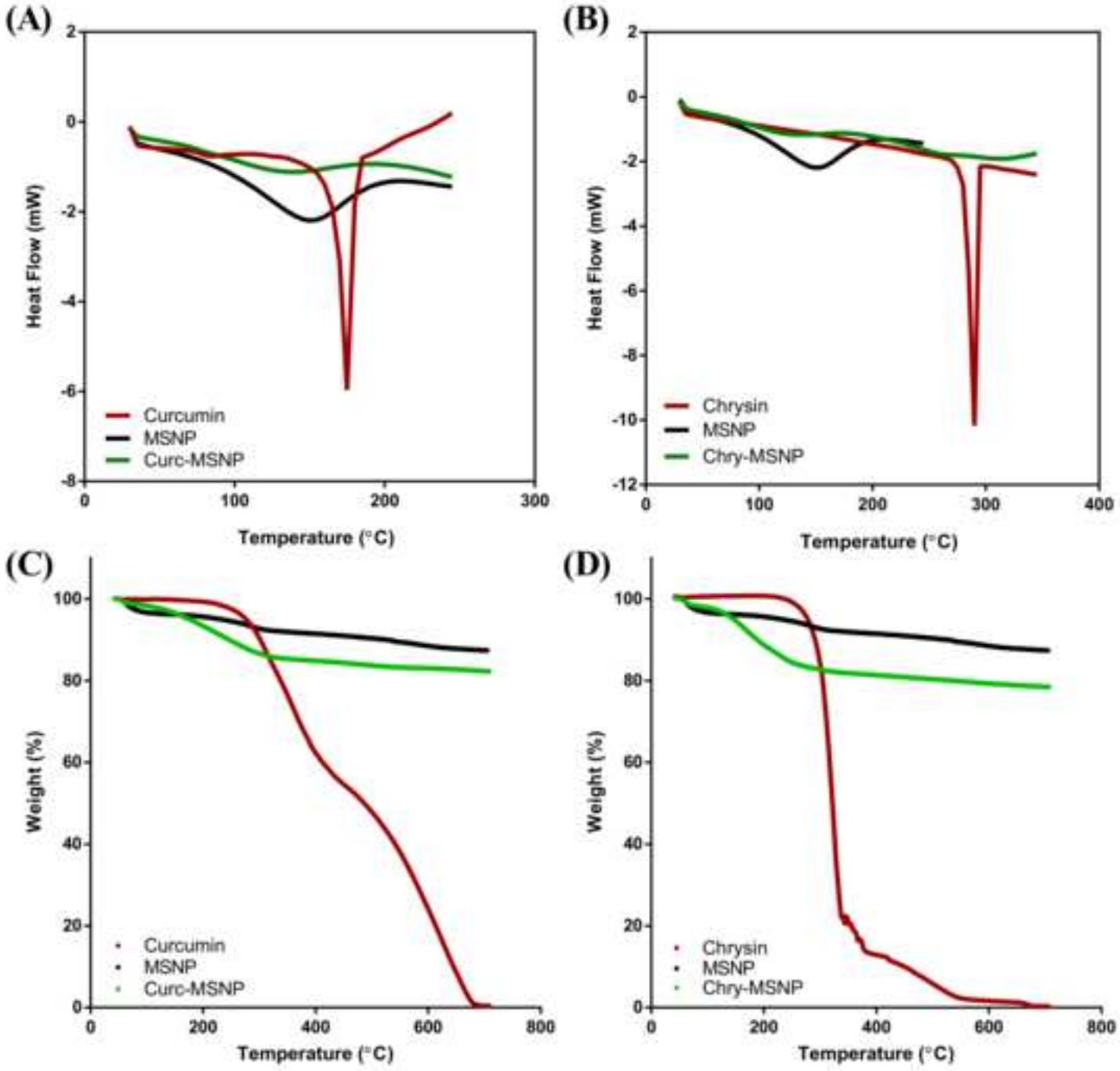
(A)
Heat Flow (mW)
Temperature (°C)
Curcumin
MSNP
Curc-MSNP
(B)
Heat Flow (mW)
Temperature (°C)
Chrysin
MSNP
Chry-MSNP
(C)
Weight (%)
Temperature (°C)
Curcumin
MSNP
Curc-MSNP
(D)
Weight (%)
Temperature (°C)
Chrysin
MSNP
Chry-MSNP

Figure 6

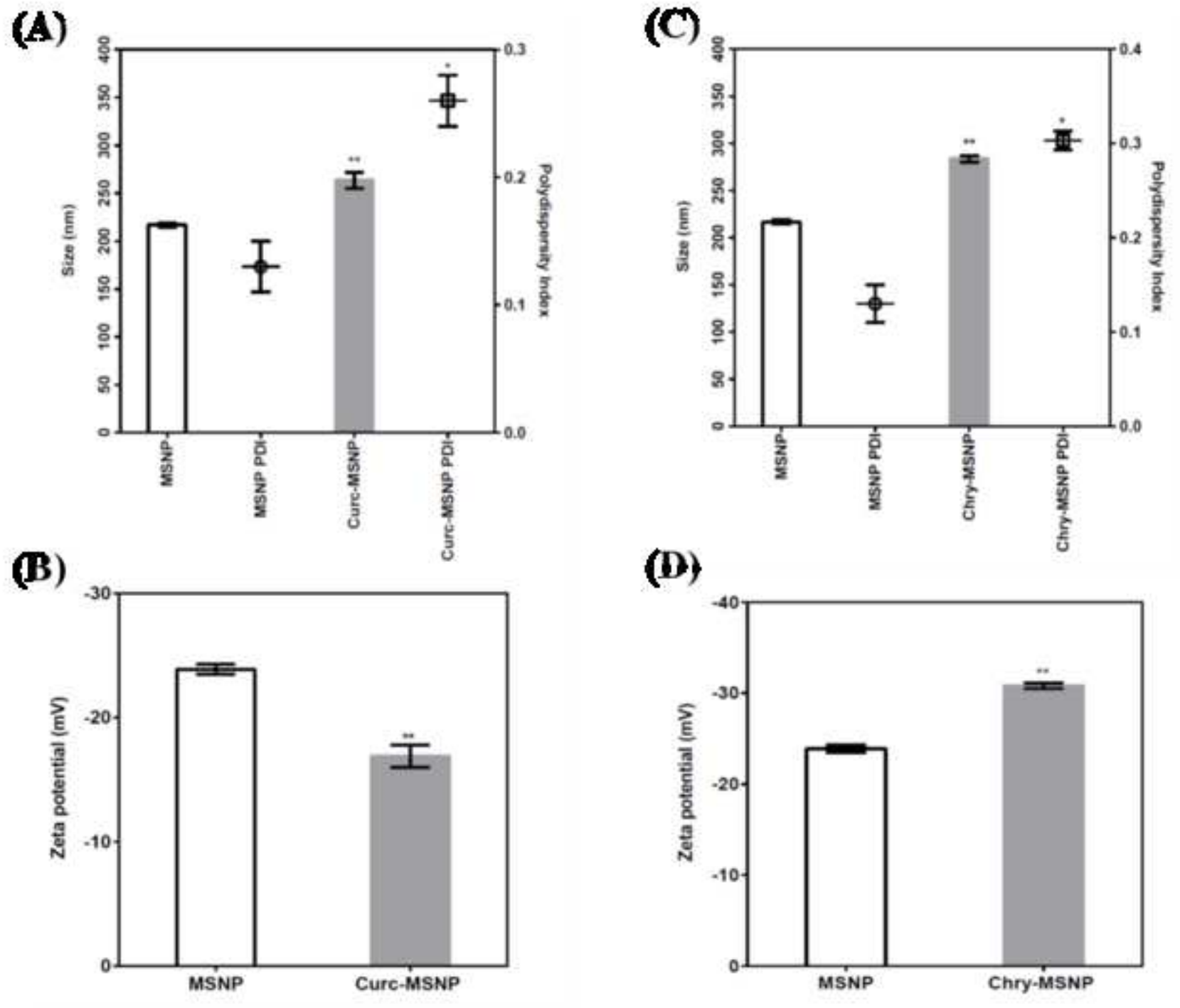
(A)
Size (nm)
Polydispersity Index
MSNP
MSNP PDI
Curc-MSNP
Curc-MSNP PDI
(B)
Zeta potential (mV)
MSNP
Curc-MSNP
(C)
Size (nm)
Polydispersity Index
MSNP
MSNP PDI
Chry-MSNP
Chry-MSNP PDI
(D)
Zeta potential (mV)
MSNP
Chry-MSNP

Figure 7

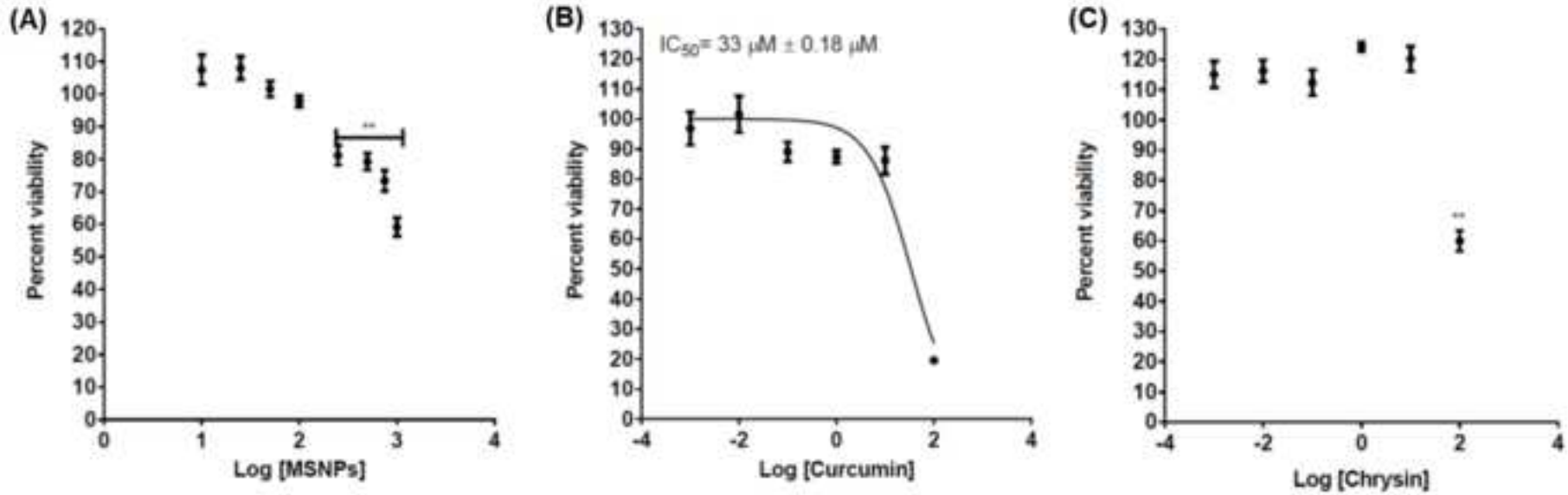
(A)
Percent viability
Log [MSNPs]
(B)
IC50= 33 μM ± 0.18 μM
Percent viability
Log [Curcumin]
(C)
Percent viability
Log [Chrysin]

Figure 8

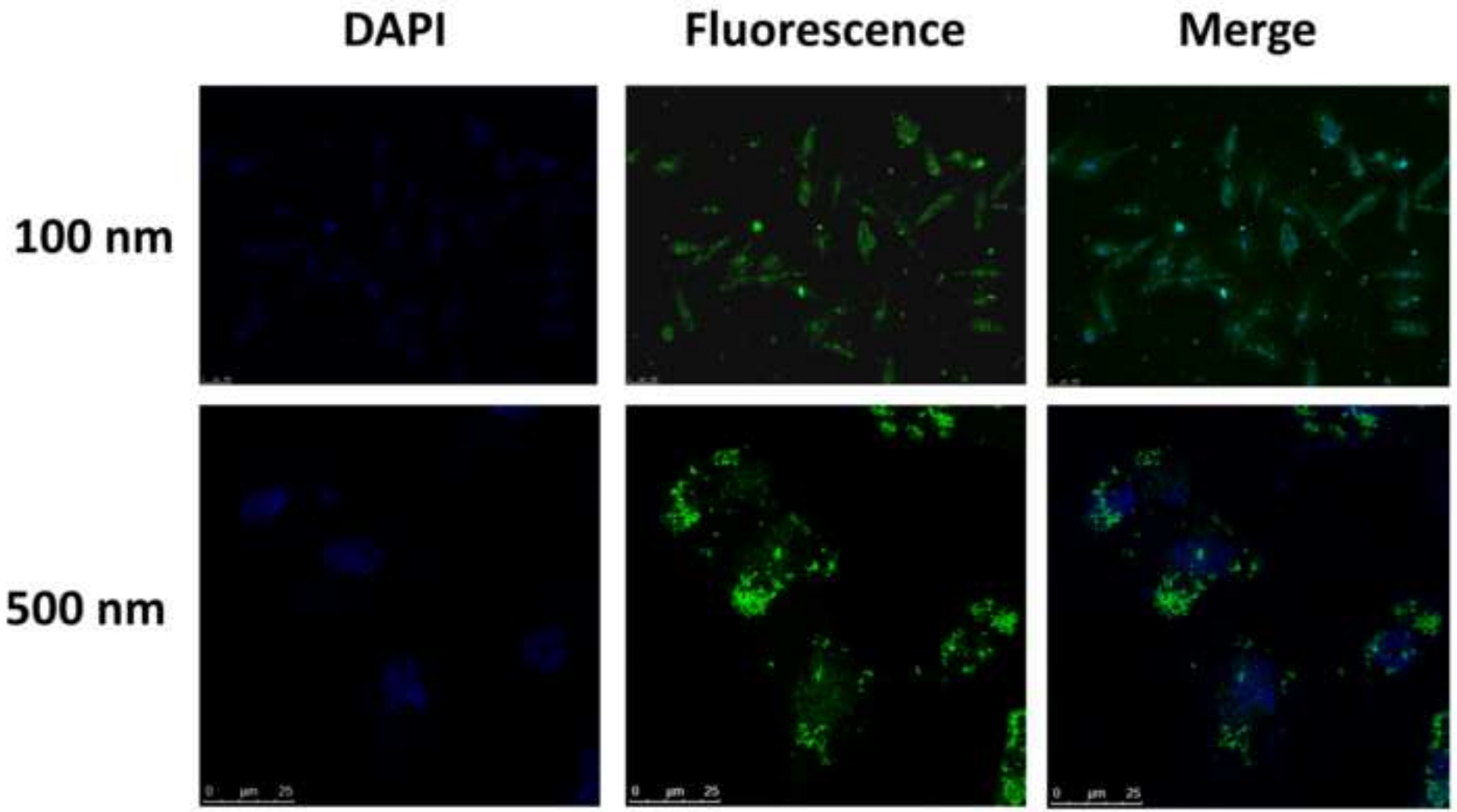

Figure 9

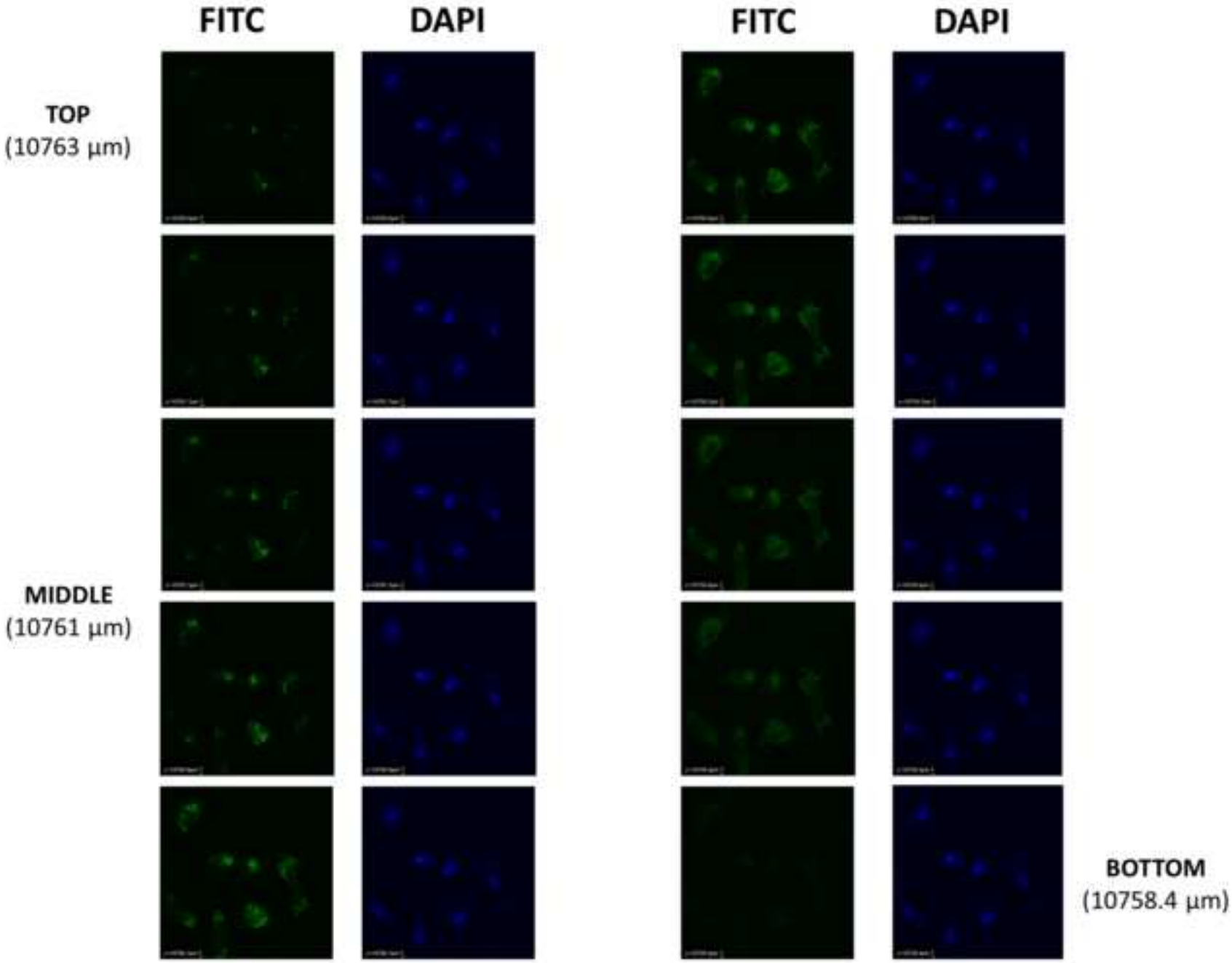
FITC
DAPI
FITC
DAPI
TOP
(10763 µm)
MIDDLE
(10761 µm)
BOTTOM
(10758.4 µm)

Figure 10

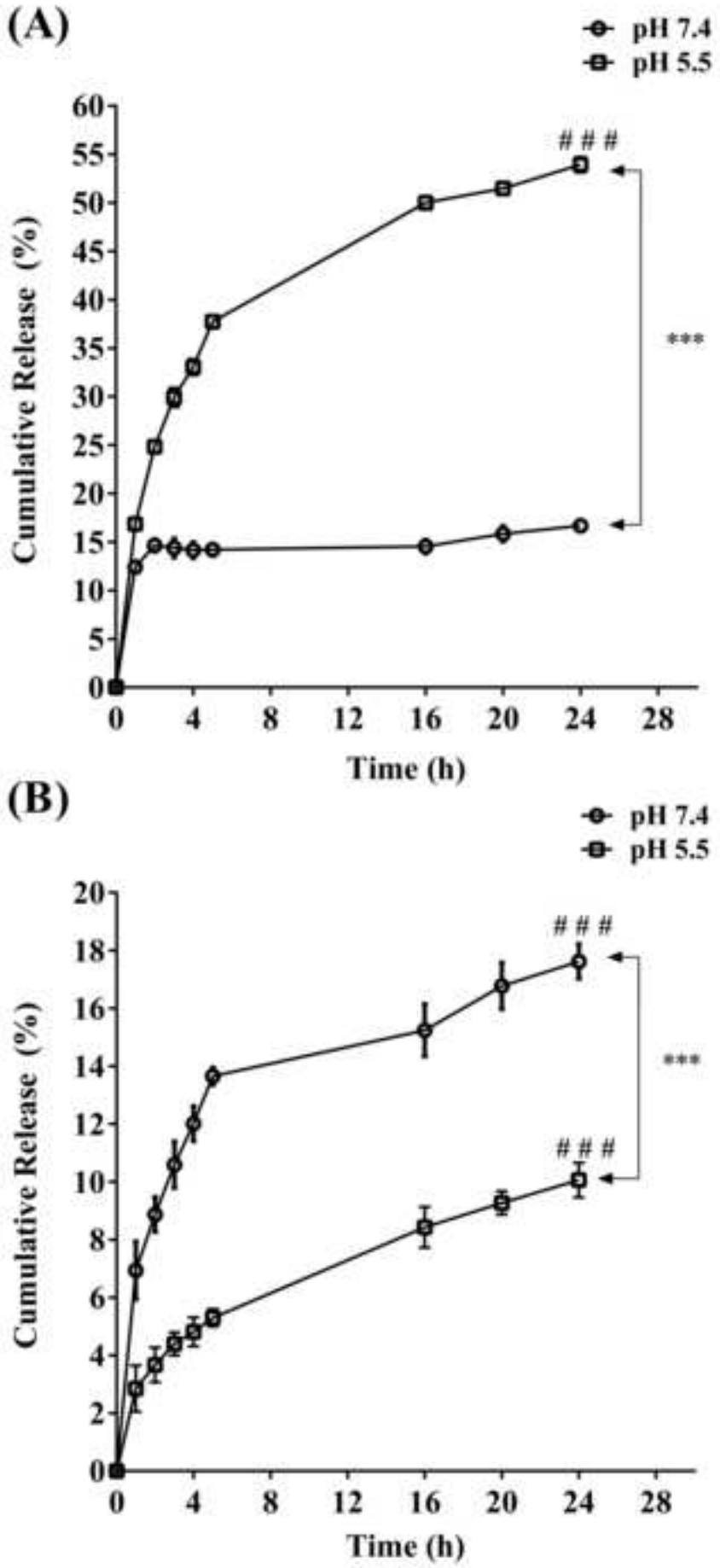
(A)
pH 7.4
pH 5.5
Cumulative Release (%)
Time (h)
###
***
(B)
pH 7.4
pH 5.5
Cumulative Release (%)
Time (h)
###
###
***